Mössbauer spectral study of the RFe$_{11.5}$Ta$_{0.5}$ (R=Tb, Dy, Ho, Er, and Lu) compounds

Cristina Piquer,* Javier Rubín, and Juan Bartolomé
Instituto de Ciencia de Materiales de Aragón-CSIC, Universidad de Zaragoza, Zaragoza, Spain

Victor Kuncser and George Filoti
Institute of Materials Science, Bucharest, Romania

(Received 25 January 2005; revised manuscript received 29 November 2005; published 25 May 2006)

The paper presents an iron-57 Mössbauer spectral study of RFe$_{11.5}$Ta$_{0.5}$, with R=Tb, Dy, Ho, Er, Lu, and an evaluation of the different contributions to the hyperfine magnetic fields. The Mössbauer spectra have been analyzed with a model that considers both the distribution of the tantalum atoms in the near-neighbor environment of the iron atoms and the relative orientation of the hyperfine field and the principal axis of the electric field gradient. Their possible directions in the ThMn$_{12}$ structure have been determined from a close examination of the point symmetry of each iron site. A local model for the hyperfine field which enables to determine their components from experimental data, has been developed and a calculation of the lattice dipolar hyperfine field in RFe$_{11.5}$Ta$_{0.5}$ has been performed. We have investigated in detail the origin and influence of the contributions to the hyperfine field coming from self 3d polarization, the iron and rare earth transferred fields and the orbital and dipolar hyperfine fields. The iron and rare earth transferred fields have been analyzed for RFe$_{11.5}$Ta$_{0.5}$ and other rare earth-iron intermetallic compounds. From this analysis it is shown that the iron transferred fields are different at each crystallographic site, and comparable to the self 3d polarization contributions, and that the rare earth transferred field is mainly originated by the indirect exchange between the rare earth 4f and iron 3d electrons.

DOI: 10.1103/PhysRevB.73.174433 PACS number(s): 75.50.Bb, 75.50.Ww, 76.80.+y

I. INTRODUCTION

Rare earth (R) iron-rich intermetallic compounds with the ThMn$_{12}$ structure (space group $I4/mmm$) have attracted great interest because they present relatively high Curie temperature, T_c, and saturation magnetization, M_s, having a crystal structure simpler than that of the R_2Fe$_{14}$B or R_2Fe$_{17}$. However, the pure RFe$_{12}$ is not stable and a nonmagnetic element M (M=Al, Si, Ti, V, Cr, Mo, W, Nb, or Ta) is needed to stabilize the ThMn$_{12}$ structure, forming the RFe$_{12-x}M_x$ pseudobinary compounds. The inclusion of the M element has a detrimental influence on both the magnetic and crystallographic properties,[1–3] consequently, one of the research lines associated with the RFe$_{12-x}M_x$compounds is the synthesis of phases with the minimal amount of stabilizing agent. We have reported on the synthesis of the series RFe$_{11.5}$Ta$_{0.5}$, with R=Tb, Dy, Ho, Er and Lu, in which the amount of the M element needed to stabilize the ThMn$_{12}$ structure is the lowest known up to date. Their crystallographic and magnetic properties have been investigated in previous works by means of x-ray diffraction, ac magnetic susceptibility, magnetization measurements, and neutron diffraction, ND.[4–6]

Following the determination of the magnetic structures of the RFe$_{11.5}$Ta$_{0.5}$ series, a ^{57}Fe Mössbauer spectral study of these compounds between T=15 and 295 K, and at T =700 K for ErFe$_{11.5}$Ta$_{0.5}$, has been carried out. The main goal of this work is to determine the different contributions to the hyperfine field, B_{hf}, in RFe$_{11.5}$Ta$_{0.5}$. There are very few works in which the components of B_{hf} are studied using experimental data. RFe$_{11.5}$Ta$_{0.5}$ provide an excellent opportunity to perform this kind of analysis, because of the consistent amount of Mössbauer and ND data that exist on the same compounds at different temperatures. This fact allows us to correlate local magnetic properties, going beyond the average bulk properties.

The organization of the paper is as follows. Section III is devoted to the fit of the Mössbauer spectra of RFe$_{11.5}$Ta$_{0.5}$ at different temperatures. Two main considerations have been taken into account: first, the random occupation of the iron 8i sites by the tantalum atoms,[5,6] which results into a binomial distribution of the tantalum near neighbors, NN, of the three crystallographic inequivalent iron sites,[7] and, second, the influence of the easy magnetization direction, EMD, on the Mössbauer spectra. It is known that B_{hf} and the principal axis of the electric field gradient, V_{zz}, can have multiple relative orientations at a given iron site, which can lead to a further splitting of the sextets given by the binomial distribution.[8–20]This additional splitting can occur independently of the compound and its consideration has been important in the analysis of the Mössbauer spectra of different R-Fe intermetallic compounds.[8–20]The main characteristics of this fitting model and the corresponding fits are presented and discussed in Sec. III A. In this section it is also shown how the different V_{zz} directions at the three crystallographic iron sites of theThMn$_{12}$ structure can be determined from the symmetry properties of each iron site. The hyperfine parameters obtained by the fit of the Mössbauer spectra are analyzed in Sec. III B, and a comparative analysis of B_{hf} and the local magnetic moments, μ_{Fe}, obtained from ND experiments is performed. The objective of this analysis is to critically revise the commonly used conversion factor approximation to transform hyperfine fields into magnetic moments.[7,21–25]

Sections IV and V are focused on the determination of the different components of B_{hf}. A local model for B_{hf} is pre-

sented and discussed in Sec. IV. The model allows us to obtain an accurate description of the relationship between B_{hf} and μ_{Fe}. Moreover, it deepens in the origin and correct modeling of the rare earth sublattice contribution to B_{hf}, the so called rare earth transferred field, B_{tR}. The study of both problems has been decoupled by analyzing separately the data of nonmagnetic and magnetic rare earth compounds in Sec. V. In Sec. V A the focus is on $LuFe_{11.5}Ta_{0.5}$, in order to obtain the different terms of B_{hf} related exclusively to the iron magnetic moments. The same procedure of data analysis is applied to other $RFe_{12-x}M_x$compounds with nonmagnetic rare earth. This analysis allows us to evaluate the contribution of the iron transferred fields to the total hyperfine field, and to understand the limitations of the conversion factor approximation. Section V B is devoted to $RFe_{11.5}Ta_{0.5}$ with magnetic rare earth in order to investigate the origin of B_{tR}. Although it is known that the rare earth may polarize the $4s$(Fe) spins, the mechanism through which this interaction takes place is not well established. This magnetic polarization can be transmitted by the Ruderman-Kittel-Kasuya-Yosida (RKKY) interaction,[26] or alternatively, by the intermediate polarization of the hybridized $5d(R)$-$3d$(Fe) band, the Campbell interaction.[27] The comparison of our results to those obtained for other R-Fe compounds allows us to check the dependence found with the lanthanide substitution with the predictions of both models. Finally, the main results of this work are summarized in Sec. VI.

II. EXPERIMENTAL

The $RFe_{11.5}Ta_{0.5}$ samples were synthesized from stoichiometric amounts of the constituent elements melted in a high-frequency induction furnace with a cold crucible. The homogeneity of the 1:12 phase was checked by x-ray diffraction, which showed small amounts of the Laves phase $TaFe_2$ and α-iron.

The ^{57}Fe Mössbauer spectra were obtained using a constant acceleration spectrometer with symmetrical wave form and a ^{57}Co source in Rh matrix. For the low temperature measurements, a set up with a closed-cycle refrigerator working down to 12 K was used, while measurements above 77 K were performed either in this set up or using a bath cryostat. Both spectrometers were calibrated at room temperature with α-iron foil. In order to improve the absorption line resolution, the thickness of the Mössbauer absorber was optimized.

The spectra were taken at different temperatures, between 15 and 290 K. In some cases two sample batches of the same compound were used. The amount of secondary phases in each sample batch were determined from x-ray data analysis and taken into account in the fitting procedure of the Mössbauer spectra.

III. MÖSSBAUER SPECTRAL MEASUREMENTS AND ANALYSIS

A. Fit of the Mössbauer spectra

In $RFe_{11.5}Ta_{0.5}$ the iron atoms occupy three inequivalent, $8i$, $8j$, and $8f$, crystallographic sites, whereas the tantalum atoms are randomly distributed only over the $8i$ sites.[5,6] As a consequence, different environments are possible for a given iron site, with probabilities given by a binomial distribution.[7] In the case of $RFe_{11.5}Ta_{0.5}$ sixteen different NN environments are possible for a given iron site. Nevertheless, due to the small contribution coming from the iron atoms with environments containing two or more NN tantalum atoms, only two contributions for each site, labeled as $8s_0$ and $8s_1$, where $s=i, j, f$, should be considered. The $8s_0$ sextet represents the contribution coming from the iron sites with zero tantalum NN, and the $8s_1$ sextet represents the average contribution coming from the iron sites with one or more tantalum NN, though it is mainly contributed by those iron sites with only one NN tantalum atom. Hence, the $8i$ sextet is subdivided into two sextets, $8i_0$and $8i_1$ with 15.61 and 14.83 percent areas, and each of the $8j$ and $8f$ sextets is subdivided into two sextets, $8j_0$ and $8j_1$, and $8f_0$ and $8f_1$, respectively, with 20.39 and 14.40 percent areas. Summarizing, at least six sextets, $8i_0$, $8i_1$, $8j_0$, $8j_1$, $8f_0$, and $8f_1$, with their relative areas fixed to the given values, are required to fit the Mössbauer spectra of $RFe_{11.5}Ta_{0.5}$.

However, a further subdivision of the two sextets assigned to each inequivalent iron site may be necessary when multiple relative orientations of V_{zz} and B_{hf} are possible at a specific iron site. The different orientations of both magnitudes can lead to different quadrupole shifts, and also may affect the hyperfine field through the anisotropic component of B_{hf}.[11–19]

The principal axis of the electric field gradient (EFG) tensor can be determined from the symmetry properties of each iron site. In the $ThMn_{12}$ structure, the $8i$ and $8j$ sites have $m2m$. point symmetry with a twofold axis parallel to the a crystallographic axis in four $8i/8j$ sites and parallel to the b crystallographic axis in the other four $8i/8j$ sites; one mirror plane is parallel to the ab plane, while the other mirror plane is parallel to either an ac plane or a bc plane. Since the components of the EFG tensor are diagonal along this twofold axis, the principal axis of the EFG in the $8i$ and $8j$ iron sites lies either along the [100] or the [010] directions, labeled as $V_{zz}^{8i,8j}$(I) and $V_{zz}^{8i,8j}$(II) in Fig. 1. The $8f$ sites have $..2/m$ point symmetry with a twofold axis parallel to a diagonal of the tetragonal plane of the structure, a mirror plane containing this twofold axis and a roto-inversion twofold axis along c. In this case the principal axis of the EFG will be along the twofold axis, that is, at ±45° respect to the a and b axes. Consequently, for one half of the $8f$ iron atoms, the principal axis is along the [110] direction, V_{zz}^{8f}(I), and for the other half, it is along the $[1\bar{1}0]$ direction, V_{zz}^{8f}(II), as it is indicated in Fig. 1. These proposed directions for V_{zz}, derived from the symmetry properties of the EFG tensor, are coincident with the principal disclination lines in the 1:12 compounds: according to Psycharis and Christides,[28] for half of the $8i$ iron atoms the principal disclination line is the [100] direction while for the other half it is the [010] direction.

The possible relative orientations of V_{zz} and B_{hf} in $RFe_{12-x}M_x$ are described in Fig. 1. For the axial magnetic phases, when the EMD is along [001], case (a) in Fig. 1, the angle θ between B_{hf} and V_{zz} is always 90°, because V_{zz} lies

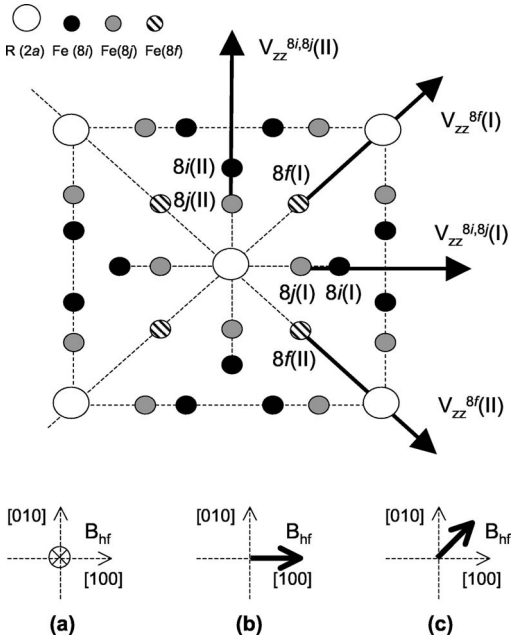

FIG. 1. The two possible directions of the principal axis, V_{zz}, of the electric field gradient tensor at the 8*i*, 8*j*, and 8*f* iron sites. (a), (b), and (c) show the different possible directions of the hyperfine field in the $ThMn_{12}$ structure.

on the *ab* basal plane of the tetragonal structure. In such a case there is no additional splitting of the six previously described sextets. When the EMD is along [100] or [010], case (b) of Fig. 1, $\theta=0°$ in four of the $8i/8j$ sites, and $\theta=90°$ for the rest of the $8i/8j$ sites. In the 8*f* sites, $\theta=\pm 45°$ for the two possible directions of V_{zz}. In this case each of the 8*i* and 8*j* contributions should be subdivided into two magnetically inequivalent sites with equal relative population, whereas no further subdivision for the 8*f* contributions is required. Consequently, ten sextets are needed to fit the total Mössbauer spectrum; labeled as $8i_0$(I), $8i_0$(II), $8i_1$(I), $8i_1$(II), $8j_0$(I), $8j_0$(II), $8j_1$(I), $8j_1$(II), $8f_0$, and $8f_1$. When the EMD lies along the [110] or $[1\bar{1}0]$ directions, case (c) in Fig. 1, each sextet assigned to the 8*f* site should be subdivided into two sextets of equal relative areas, whereas the 8*i* and 8*j* sites will not show additional splitting. Then, the spectra should be modeled with an eight sextets fitting function. The corresponding sextets will be labeled as $8i_0$, $8i_1$, $8j_0$, $8j_1$, $8f_0$(I), $8f_0$(II), $8f_1$(I), and $8f_1$(II). Finally, for intermediate orientation of the EMD, i.e., canted magnetic phases, the situation is similar, but the angles are different. This kind of sextet subdivision has been successfully applied in the study of $R\mathrm{Fe}_{11}\mathrm{Ti}$ and $R\mathrm{Fe}_{11}\mathrm{TiH}$,[14–19,29–31] and it is also well established for $R_2\mathrm{Fe}_{17}$,[11,12] $R\mathrm{Fe}_6\mathrm{Ge}_6$,[13] or $R\mathrm{Fe}_2$.[8–10] In $R\mathrm{Fe}_{11}\mathrm{Ti}$ and $R\mathrm{Fe}_{11}\mathrm{TiH}$, in order to reduce the number of adjustable parameters, it has been assumed a linear dependence of the hyperfine parameters on the number of titanium NN. In $R\mathrm{Fe}_{11.5}\mathrm{Ta}_{0.5}$, since there are just 0.5 tantalum atoms per formula unit, only two sextet per site are necessary, and the linear approximation is no longer necessary.

Summarizing, three different fitting models are proposed for $R\mathrm{Fe}_{11.5}\mathrm{Ta}_{0.5}$. In the six sextets model eighteen hyperfine parameters, one linewidth, and one total absorption area are involved in the fit. When the Mössbauer spectra are modeled with ten sextets, twenty six hyperfine parameters, one linewidth, and one total absorption area are involved. Alternatively, twenty two hyperfine parameters, one linewidth, and one total absorption area are needed in the eight sextets model. In the last two cases it has been considered that since the magnetically inequivalent pairs are crystallographically equivalent, their isomer shifts should be identical.[11] The validity of these models with such large number of adjustable parameters will be checked from the goodness of the fit and by the requirement of physically reasonable hyperfine parameters including thermal and site dependencies.

In all the studied compounds the assignment of the sextets to the different crystallographic sites is based upon their relative intensities, isomer shifts, δ, and B_{hf}. Specifically, it is known that a larger Wigner-Seitz volume leads to a more positive iron isomer shift.[11] In $R\mathrm{Fe}_{11.5}\mathrm{Ta}_{0.5}$ the Wigner-Seitz cell volumes follow the sequence $V(8i)>V(8j)>V(8f)$, which sets the isomer shift sequence $\delta(8i)>\delta(8j)>\delta(8f)$.[32,33] The hyperfine fields are expected to follow the sequence of the magnetic moment values. It is known from previous ND experiments that the iron magnetic moments follow the trend $\mu_{Fe}(8i)>\mu_{Fe}(8j)\geqslant\mu_{Fe}(8f)$.[6] Consequently, the sextets with the highest isomer shift and hyperfine field are assigned to the 8*i* site, both on the basis of its percent contribution and its iron NN environment. Such criterium is not suitable to discriminate between the 8*j* and 8*f* sites since they contribute to the Mössbauer spectrum with the same relative area and their magnetic moments are similar; therefore, the assignment is based only on the isomer shifts.

The amount of impurities, such as magnetic α-iron or paramagnetic $TaFe_2$, were determined by x-ray analysis. Since their hyperfine parameters are known from literature,[34] they were included in the fit as additional patterns with no modification of the number of adjustable parameters.

The quadrupole shift, ε, is defined as the absolute value of the energy shift of the nuclear excited levels when the quadrupole interaction is treated as a first-order perturbation to the magnetic interaction[35,36]

$$\varepsilon=\frac{eQV_{zz}}{4}\left(\frac{3\cos^2\theta-1+\eta\sin^2\theta\cos 2\phi}{2}\right), \qquad (1)$$

where *e* is the electron charge, *Q* the iron nuclear quadrupole moment, V_{zz} the principal component of the EFG, η the asymmetry parameter, and θ and ϕ the polar and azimuthal angles of the hyperfine field direction with respect to the EFG frame of reference.

In all cases the estimated errors of the obtained hyperfine parameters are at most ±0.3 T for the hyperfine fields, ±0.020 mm/s for the isomer shifts and ±0.050 mm/s for the quadrupole shifts. The observed linewidths were typically of 0.38 ± 0.02 mm/s for all the compounds, a value slightly larger than the experimental calibration linewidth of 0.28 mm/s. This broadening has also been reported for $R\mathrm{Fe}_{11}\mathrm{Ti}$ and $R\mathrm{Fe}_{11}\mathrm{TiH}$,[14–19,30,31] and, very probably, is due to a non-negligible contribution of the second neighbor shell,

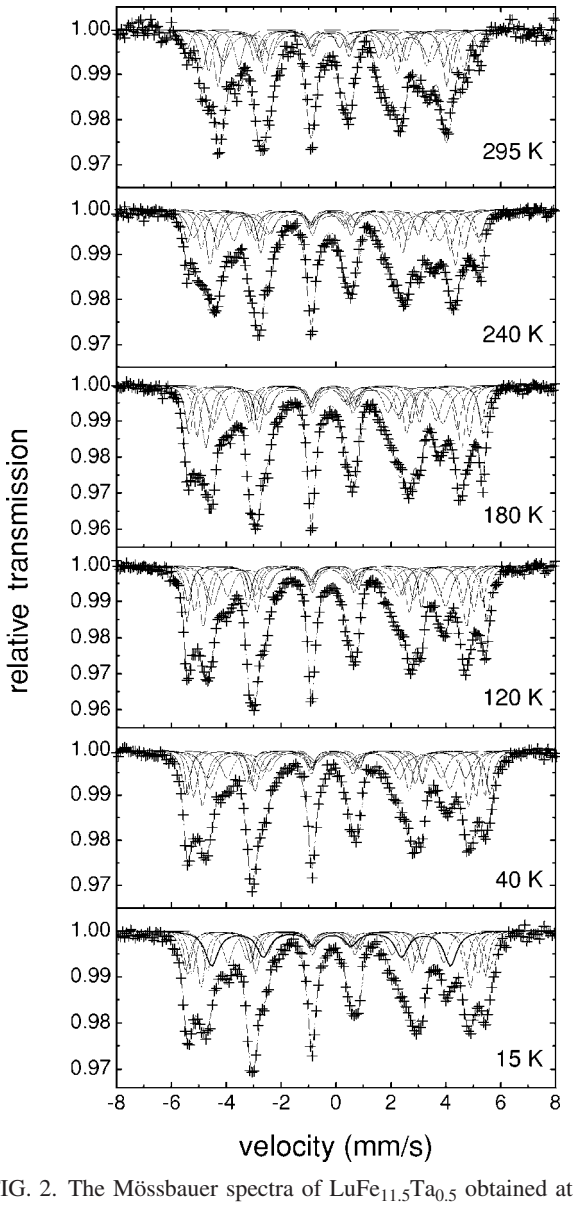

FIG. 2. The Mössbauer spectra of $LuFe_{11.5}Ta_{0.5}$ obtained at the indicated temperatures.

and also to slight deviations from the nominal stoichiometry or to any possible tantalum spatial inhomogeneity.

1. $LuFe_{11.5}Ta_{0.5}$ *and* $HoFe_{11.5}Ta_{0.5}$

Both compounds show axial EMD from 1.5 K to T_c.[4,6] Consequently, their Mössbauer spectra were fit with the six sextets model described in Sec. III A. The spectra of $LuFe_{11.5}Ta_{0.5}$ reveal the presence of a 10% α-iron, in agreement with the amount of impurity determined from x-ray diffraction. As is shown in Figs. 2 and 3, all the fits are very good, showing the adequacy of the model. The corresponding hyperfine parameters are given in Tables I and II.

The site weighted average hyperfine fields and isomer shifts, $B_{hf}(k)$ and $\delta(k)$, $k=8i$, $8j$, and $8f$, and the total average hyperfine field and isomer shift, $\langle B_{hf}\rangle$ and $\langle\delta\rangle$, are plotted as a function of the temperature in Figs. 4 and 5. In all cases the weight is the relative area of the sextets associated to each site.

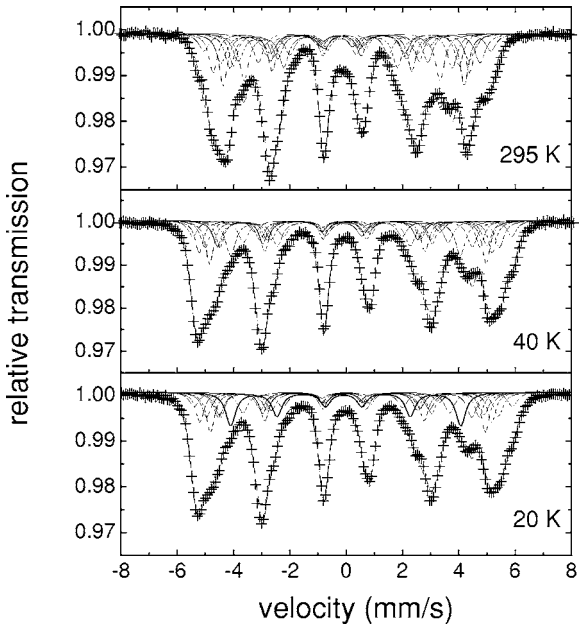

FIG. 3. The Mössbauer spectra of $HoFe_{11.5}Ta_{0.5}$ obtained at the indicated temperatures.

2. $ErFe_{11.5}Ta_{0.5}$

The Mössbauer spectra of $ErFe_{11.5}Ta_{0.5}$ has been measured between 15 and 295 K, and also at $T=700$ K, when the compound is in the paramagnetic phase, $T_c=532$ K.[4,6] The Er compound shows a spin reorientation transition, SRT, at $T_s\approx 40$ K, from an axial (above T_s) to a canted magnetic phase (below T_s) in which the EMD deviates by an angle θ_c from the crystallographic c axis.[4,6] The measurements above and below T_s were performed on different batches. The sample measured at $T=15$ and 30 K contained a small amount of $TaFe_2$ impurity phase, which corresponds to the doublet of $\approx 3\%$ of relative area included in the fit.

At $T>T_c$, the paramagnetic Mössbauer spectrum was fit with three symmetric doublets with relative intensities 3.5:4:4, see Fig. 6. These three doublets correspond to the average contributions of the three iron sites $8i$, $8j$, and $8f$, respectively, and the corresponding hyperfine parameters are given in Table III. It is also possible to fit the paramagnetic spectra using six symmetric doublets, with relative areas fixed to the values used for the six sextets model. However, in such a case, the overlap of the paramagnetic doublets is rather high and it is not possible to obtain reliable fits with such a number of adjustable parameters. The spectra taken at temperatures below T_c and above T_s were successfully fit with the six sextets model, see Fig. 6. Below T_s, a further subdivision of the two sextets assigned to each inequivalent iron sites was necessary to obtain good fits, and the eight and ten sextets models described in Sec. III A were tried. The eight sextets fit gave very large and unrealistic linewidths of about 0.60 mm/s. Furthermore, the misfit parameter of the ten sextets fit, 0.3%, is significantly lower than the misfit parameter obtained using the eight sextets model, 0.8%. That is, at $T<T_s$ the Mössbauer spectra is consistent with an EMD contained in the (100) or (010) planes. This result is similar to that found for $ErFe_{11}Ti$ and $ErFe_{11}TiH$,which un-

TABLE I. Mössbauer hyperfine parameters for $LuFe_{11.5}Ta_{0.5}$.

Parameter	T, K	$8i_0$	$8i_1$	$8j_0$	$8j_1$	$8f_0$	$8f_1$	Total wt. aver.
B_{hf},T	290	30.3	28.3	25.8	24.9	23.4	21.2	25.5
	240	32.3	29.9	27.9	26.5	25.0	22.4	27.2
	180	33.4	30.9	29.0	27.9	25.9	23.4	28.4
	120	34.0	31.7	29.9	28.8	26.5	24.0	29.1
	80	34.3	32.1	30.3	29.2	26.7	24.3	29.5
	40	34.4	32.0	30.3	29.3	27.0	24.4	29.5
	15	34.6	32.5	30.6	29.3	27.1	24.5	29.7
δ,[a] mm/s	290	0.030	−0.050	−0.036	−0.179	−0.147	−0.146	−0.086
	240	0.075	−0.017	−0.015	−0.083	−0.100	−0.105	−0.041
	180	0.097	0.006	0.020	−0.042	−0.089	−0.071	−0.014
	120	0.116	0.031	0.049	−0.014	−0.091	−0.060	0.003
	80	0.123	0.045	0.063	0.009	−0.074	−0.021	0.022
	40	0.141	0.058	0.086	0.007	−0.045	−0.011	0.038
	15	0.130	0.064	0.080	0.014	−0.035	−0.004	0.041
ε, mm/s	290	0.024	−0.005	0.011	0.098	−0.027	0.071	0.024
	240	0.020	0.021	0.018	0.123	−0.036	0.088	0.033
	180	0.036	0.013	0.018	0.116	−0.055	0.091	0.030
	120	0.037	0.026	0.030	0.119	−0.036	0.085	0.037
	80	0.038	0.024	0.036	0.104	-0.028	0.100	0.040
	40	0.054	0.027	0.027	0.117	−0.037	0.078	0.038
	15	0.047	0.029	0.036	0.126	-0.026	0.115	0.048

[a]Relative to α-iron at 295 K.

dergo the same kind of SRT at low temperatures.[14] The fits with the ten sextets model and the resulting hyperfine parameters are displayed in Fig. 6 and Table IV, respectively. The temperature dependence of $B_{hf}(k)$, $\langle B_{hf}\rangle$, $\delta(k)$, and $\langle\delta\rangle$ are shown in Fig. 7.

The measurements performed at $T=700$ K allow to compare the hyperfine parameters in the ordered and paramagnetic regions. As we can see from Fig. 7, the isomer shifts at $T=700$ K follow the same sequence, $\delta(8i)>\delta(8j)>\delta(8f)$, than in the ordered state, and their temperature dependence can satisfactorily be fit with the Debye model for the second-order Doppler shift, see Sec. III B. At $T=700$ K, the paramagnetic doublets are characterized by the quadrupole splitting, $\Delta E_Q=\frac{eQV_{zz}}{2}(1+\eta^2/3)^{1/2}$. However, the ΔE_Q values should be compared with caution with the ε values obtained in the axial magnetic case. First, the ΔE_Q values obtained at $T=700$ K are average values, and, second, due to a nonzero asymmetry parameter the ε values in the axial magnetic phases can be smaller than those expected for the $\eta=0$ case. For instance, an asymmetry parameter of about 0.4 would explain the experimental values of ε.

3. $DyFe_{11.5}Ta_{0.5}$

In the Dy compound two SRTs take place at $T_{s1}\approx 265$ K and $T_{s2}\approx 210$ K.[4,6] At $T=T_{s1}$ the magnetization direction ro-

TABLE II. Mössbauer hyperfine parameters for $HoFe_{11.5}Ta_{0.5}$.

Parameter	T, K	$8i_0$	$8i_1$	$8j_0$	$8j_1$	$8f_0$	$8f_1$	Total wt. aver.
B_{hf},T	290	30.5	28.2	26.6	25.4	24.1	21.0	26.0
	40	35.1	32.2	32.2	30.3	27.9	25.4	30.5
	15	35.2	32.4	32.3	30.5	28.1	25.3	30.6
δ,[a] mm/s	290	0.022	0.001	−0.107	−0.116	−0.161	−0.171	−0.092
	40	0.134	0.090	0.012	0.002	−0.045	−0.055	0.020
	15	0.135	0.092	0.015	0.005	−0.042	−0.052	0.022
ε, mm/s	290	0.220	0.310	−0.039	0.131	0.012	0.052	0.100
	40	0.168	0.251	−0.064	0.109	0.011	0.060	0.077
	15	0.231	0.266	−0.047	0.123	0.018	0.073	0.098

[a]Relative to α-iron at 295 K.

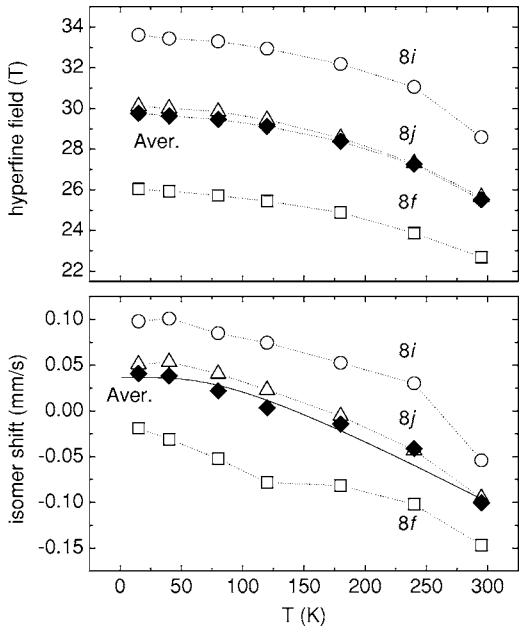

FIG. 4. Top panel: the temperature dependence of the three site weighted average hyperfine fields in $LuFe_{11.5}Ta_{0.5}$: $8i$ (○), $8j$ (△), and $8f$ (□) and the total average hyperfine field (◆). Bottom panel: the temperature dependence of the three site weighted average isomer shifts in $LuFe_{11.5}Ta_{0.5}$: $8i$ (○), $8j$ (△), and $8f$ (□) and the total average isomer shift (◆). The solid line through the total average isomer shift is the result of a fit with a Debye model of the second-order Doppler shift.

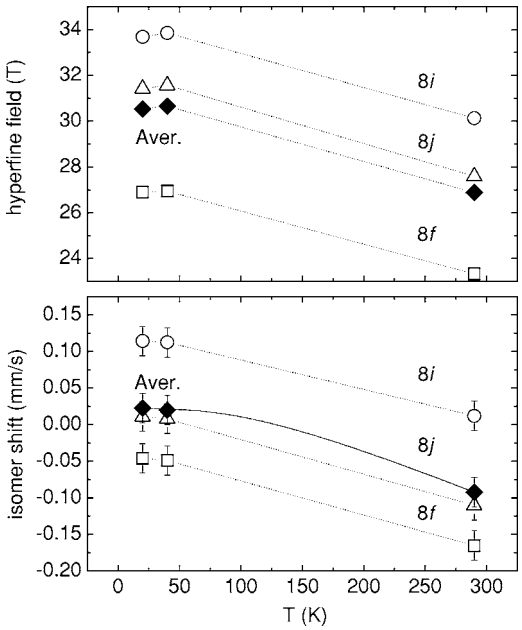

FIG. 5. Top panel: the temperature dependence of the three site weighted average hyperfine fields in $HoFe_{11.5}Ta_{0.5}$: $8i$ (○), $8j$ (△), and $8f$ (□) and the total average hyperfine field (◆). Bottom panel: the temperature dependence of the three site weighted average isomer shifts in $HoFe_{11.5}Ta_{0.5}$: $8i$ (○), $8j$ (△), and $8f$ (□) and the total average isomer shift (◆). The solid line through the total average isomer shift is the result of a fit with a Debye model of the second-order Doppler shift.

tates away from the room temperature EMD (c axis) to a canted magnetic structure ($\theta_c=44°$ at $T=250$ K), and at $T=T_{s2}$, the EMD reaches the basal plane of the tetragonal structure.[4,6]

The Mössbauer spectrum at 295 K was straightforwardly fit with the six sextets model and with a doublet for a small amount, ≈2% of relative area, of $TaFe_2$ secondary phase. When the compound is in the basal magnetic phase, $T<210$ K, a further subdivision of the initial six sextets should be considered, and the eight and ten sextets models were tried. The fits obtained by applying the ten sextets model were considered better than those obtained with the eight sextets model on the basis of their corresponding misfit parameters: 0.4% for the ten sextets model and 0.7% for the eight sextets model. Besides, there is a nice confirmation of this result in the shape of the Mössbauer spectra, see Fig. 8. At $T=295$ K, when the compound is in an axial magnetic phase, the greater hyperfine field corresponds to the $8i_0$ sextet, which is the responsible for the most external peaks, at −5.4 and 5.1 mm/s. At $T<295$ K, when the compound is in its basal magnetic phase, these most external peaks have reduced their intensity by a factor of two, which is in perfect agreement with the splitting of the $8i_0$ contribution into $8i_0$(I) and $8i_0$(II) predicted by the ten sextets model. Consequently, the Mössbauer spectra of $DyFe_{11.5}Ta_{0.5}$ in its basal magnetic phase are compatible with the EMD oriented along the [100] or [010] directions.

This result is similar to that found in the analysis of the Mössbauer spectra of $DyFe_{11}Ti$ and $DyFe_{11}TiH$.[14] However, it seems to be in disagreement with the work of Algarabel *et al.*, who have found that the EMD of the $DyFe_{11}Ti$ is along the [110] direction.[37] The origin of such discrepancies probably lies in the fact the magnetocrystalline properties of the $RFe_{12-x}M_x$ compounds are very sensitive to the nature and content of the M element, especially for R=Dy and Tb.[38–40]

The fits with the six and ten sextets models are presented in Fig. 8, and the obtained hyperfine parameters are displayed in Table V. The temperature dependence of $B_{hf}(k)$, $\langle B_{hf}\rangle$, $\delta(k)$, and $\langle\delta\rangle$ are shown in Fig. 9.

4. $TbFe_{11.5}Ta_{0.5}$

$TbFe_{11.5}Ta_{0.5}$ exhibits basal EMD in the temperature range 4.2 K-T_c.[4,6] The eight and ten sextets fitting models gave similar hyperfine parameters, and also similar misfit parameters (≈0.4%). The main difference between both fits is that the ten sextets model gave unrealistic linewidths, larger than 0.75 mm/s. Since the eight sextet model gives linewidths of ≈0.37 mm/s, it is concluded that the Mössbauer spectra of $TbFe_{11.5}Ta_{0.5}$ are better described assuming that the EMD is along [110].

This result seems to be in disagreement with the EMD reported for $TbFe_{11}Ti$, [100],[17,41] but it should be noted that each compound present a different magnetic phase diagram; $TbFe_{11.5}Ta_{0.5}$ displays basal EMD over the whole temperature range, whereas $TbFe_{11}Ti$ undergoes a SRT from an axial to a basal magnetic phase at $T\approx 338$ K.[17] As in $DyFe_{11.5}Ta_{0.5}$, these differences are very probably due to the fact that the magnetocrystalline properties of the $TbFe_{12-x}M_x$ compounds are very sensitive to the nature and content of the

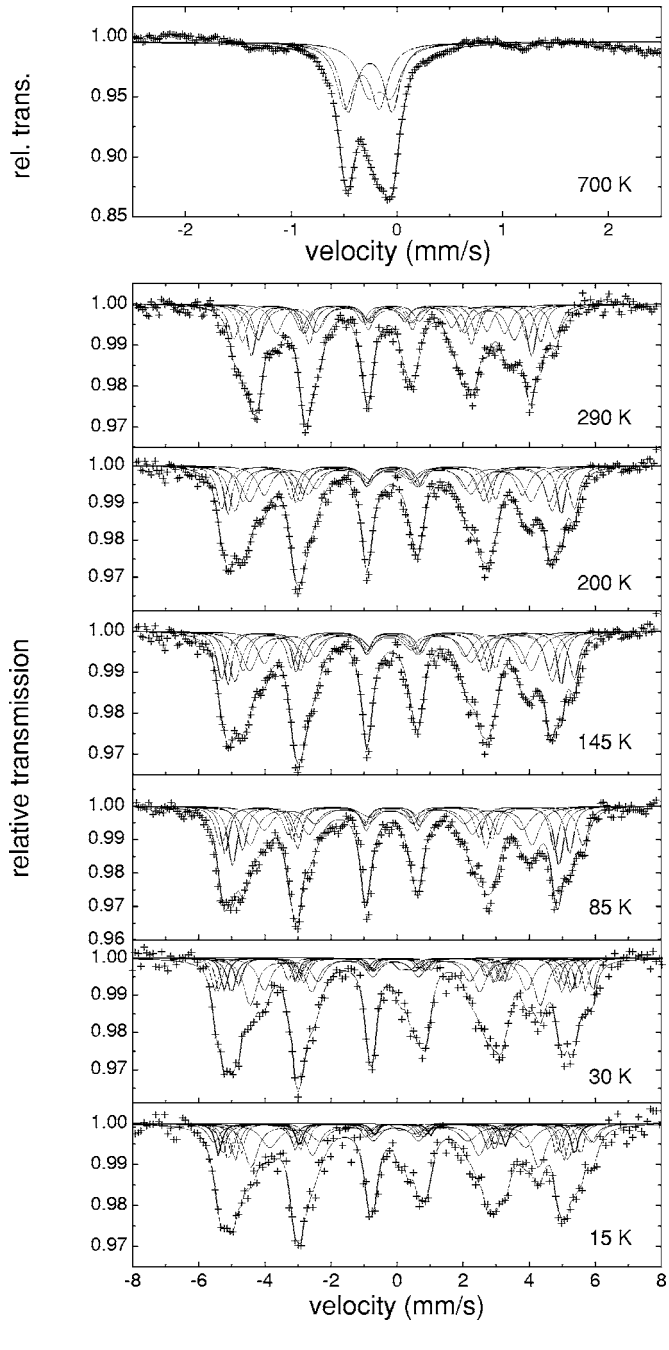

FIG. 6. The Mössbauer spectra of $ErFe_{11.5}Ta_{0.5}$ obtained at the indicated temperatures.

M element.[38–40] In particular, it has been observed in $TbFe_{12-x}Ti_x$ that when the Ti concentration is decreased, there is an increase in the SRT temperature and the EMD in the basal plane changes from [100] to [110].[39]

The fits with the eight sextets model are shown in Fig. 10. The fitted hyperfine parameters are displayed in Table VI, and the thermal dependence of $B_{hf}(k)$, $\langle B_{hf}\rangle$, $\delta(k)$, and $\langle\delta\rangle$ are presented in Fig. 11.

B. Analysis of the hyperfine parameters

In all measured compounds it was observed that the changes in the hyperfine field upon the replacement of one iron by one tantalum as NN range between −1.5 and −3.0 T, see Tables I–VI. This modification of the hyperfine field seems to be characteristic of the $RFe_{12-x}M_x$ structure, because a very similar reduction of the hyperfine field, between −1.5 and −3.5 T, has been observed when substituting one iron by one titanium in $RFe_{11}Ti$.[14–19,29–31] In the nonaxial magnetic phases the differences between the hyperfine fields assigned to each pair of magnetically inequivalent sites, B_{hf}(I) and B_{hf}(II), range between 0.1 and 3.7 T, see Tables I–VI, very similar to those found in the analysis of R_2Fe_{17} and $RFe_{11}Ti$.[11,12,14–19] These differences come from the anisotropic contributions to B_{hf}, which depend on the relative orientation of the EMD and V_{zz}.[42,43] The obtained values for $|B_{hf}(\mathrm{I})\text{-}B_{hf}(\mathrm{II})|$ agree with the results of Averbuch-Pouchot *et al.*, who have observed differences in the anisotropic part of B_{hf} of about 1–3 T for differences of 90° between the EMD and the V_{zz} directions in Y_2Fe_{17}.[42]

The temperature dependence of the total average isomer shift, $\langle\delta\rangle$, has been fit with the Debye model for the second-order Doppler shift,[44,45] solid lines in Figs. 4, 5, 7, 9, and 11. In all cases the resulting iron effective vibrating mass[44] is 57 g/mol, and the effective Mössbauer temperatures are 364, 346, 393, 400, and 358 (±10) K, for R =Tb, Dy, Ho, Er and Lu, respectively. These temperatures are typical of intermetallic compounds.[14–19,30,31,46,47] We have obtained that, in general, the isomer shift decreases upon the replacement of one iron by one tantalum as near neighbor for the 8i and 8j sites, whereas the Ta substitution has a minor effect for the 8f site. The only exception to this behavior seems to be $TbFe_{11.5}Ta_{0.5}$; in this compound the 8f isomer shift decrease per tantalum atom is around −0.100 mm/s, greater than the decrease observed for the 8i and 8$j$sites. Similar values have been found in $RFe_{11}Ti$.[14–19,29–31] The observed quadrupole shifts, ε, in the $RFe_{11.5}Ta_{0.5}$ are relatively small and lie between −0.173 and 0.310 mm/s, see Tables I–VI.

The site weighted average hyperfine fields, $B_{hf}(k)$, k=8i, 8j, and 8f, can be used to analyze their relationship with the local magnetic moments, $\mu_{Fe}(k)$, obtained from a previous ND study.[6] In particular, they can be used to revise the commonly used conversion factor approximation to relate hyperfine fields to magnetic moments.

TABLE III. Mössbauer hyperfine parameters for $ErFe_{11.5}Ta_{0.5}$ at T=700 K.

Parameter	T, K	8i site aver.	8j site aver	8f site aver.	Total wt. aver.
δ,[a] mm/s	700	−0.231	−0.373	−0.496	−0.373
ΔE_Q, mm/s	700	0.305	0.642	0.492	0.487

[a]Relative to α-iron at 295 K.

TABLE IV. Mössbauer hyperfine parameters for $ErFe_{11.5}Ta_{0.5}$. The symbol–indicates identical values for (I) and (II) sites.

Parameter	T, K	$8i_0$(I)	$8i_0$(II)	$8i_1$(I)	$8i_1$(II)	$8j_0$(I)	$8j_0$(II)	$8j_1$(I)	$8j_1$(II)	$8f_0$	$8f_1$	Total wt. aver.
B_{hf}, T	290	30.1	–	27.9	–	26.3	–	25.2	–	24.0	21.2	25.7
	200	32.7	–	30.8	–	28.9	–	27.7	–	25.6	23.3	28.1
	145	33.3	–	31.5	–	29.9	–	28.9	–	26.6	24.4	29.0
	85	34.2	–	32.5	–	30.8	–	29.4	–	26.6	24.3	29.6
	30	35.3	35.0	33.3	32.8	32.0	31.2	30.7	30.1	27.4	24.8	30.4
	18	35.8	34.7	33.6	33.0	31.7	31.4	30.6	30.1	27.1	24.1	30.3
δ,[a] mm/s	290	0.041	–	−0.070	–	−0.062	–	−0.143	–	−0.148	−0.142	−0.088
	200	0.087	–	−0.006	–	0.000	–	−0.070	–	−0.124	−0.109	−0.038
	145	0.087	–	0.021	–	−0.005	–	−0.026	–	−0.095	−0.034	−0.005
	85	0.136	–	0.055	–	0.027	–	0.020	–	-0.064	−0.042	0.017
	30	0.145	–	0.081	–	0.043	–	−0.001	–	−0.040	−0.063	0.026
	18	0.171	–	0.083	–	0.051	–	0.022	–	−0.040	−0.028	0.029
ε, mm/s	290	0.007	–	0.027	–	0.018	–	0.141	–	−0.062	0.075	0.027
	200	0.072	–	0.047	–	0.038	–	0.112	–	−0.009	0.051	0.047
	145	0.064	–	0.030	–	0.023	–	0.073	–	0.016	0.043	0.039
	85	0.066	–	0.038	–	0.029	–	0.074	–	0.003	0.024	0.036
	30	0.142	−0.026	0.052	−0.038	0.083	−0.040	0.141	0.030	−0.007	0.026	0.029
	18	0.034	0.127	−0.091	0.066	−0.021	0.150	−0.105	0.097	−0.014	0.055	0.028

[a]Relative to α-iron at 295 K.

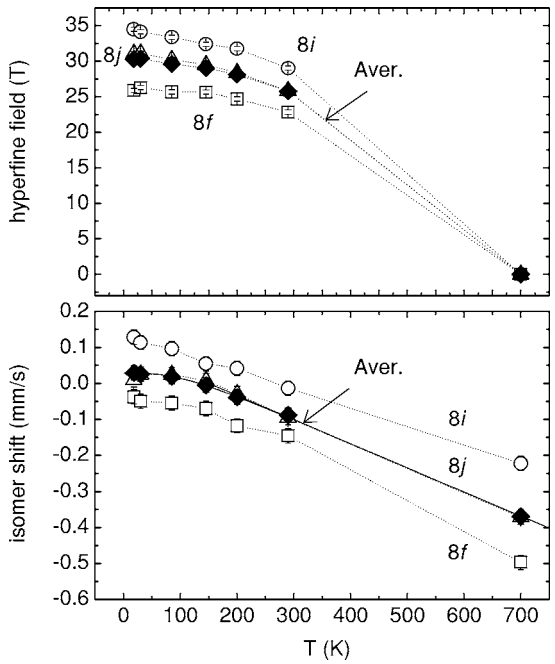

FIG. 7. Top panel: the temperature dependence of the three site weighted average hyperfine fields in $ErFe_{11.5}Ta_{0.5}$: $8i$ (○), $8j$ (△), and $8f$ (□) and the total average hyperfine field (♦). Bottom panel: the temperature dependence of the three site weighted average isomer shifts in $ErFe_{11.5}Ta_{0.5}$: $8i$ (○), $8j$ (△), and $8f$ (□) and the total average isomer shift (♦). The solid line through the total average isomer shift is the result of a fit with a Debye model of the second-order Doppler shift.

In the $RFe_{12-x}M_x$, and in other R-Fe intermetallic compounds, it is usually assumed that the iron magnetic moments can be estimated from hyperfine fields by applying a constant conversion factor, f.[7,21–25] As already noticed by Coehoorn *et al.* this procedure is probably based on the fact that there is a large number of Y-Fe binary compounds in which the ratio between the *average* hyperfine field, $\langle B_{hf}\rangle$, and the *average* magnetic moment, $\langle \mu_{Fe}\rangle$, is almost constant, $f=14.8\ \mathrm{T}/\mu_B$.[48] However, this approximation can result in substantial errors when it is used to determine the iron magnetic moments at the different crystallographic sites, $\mu_{Fe}(k)$. In particular, in $RFe_{11.5}Ta_{0.5}$ the magnetic moments calculated as $\mu_{Fe}(k)=B_{hf}(k)/14.8$ can differ by more than 30% from the magnetic moments obtained from ND experiments. This difference appears because the ratio $f_k=B_{hf}(k)/\mu_{Fe}(k)$ can be significatively different for each crystallographic iron site, see, for instance, Table VII. For $RFe_{11.5}Ta_{0.5}$ the ratio f_k ranges between 13.3 and 17.0 T/μ_B, and between 10.2 and 17.4 T/μ_B for other $RFe_{12-x}M_x$ compounds.[15,21,26,49–53] Moreover, the ratio $\langle f\rangle=\langle B_{hf}\rangle/\langle \mu_{Fe}\rangle$ can be different depending on the compound, see Table VII. Similar results have been found even in binary Y-Fe compounds; for instance, Coehoorn *et al.* have observed that the ratio between $B_{hf}(k)$ and $\mu_{Fe}(k)$ ranges between 11.6 and 15.0 T/μ_B for the different k crystallographic sites of Y_6Fe_{23},[48] and Beuerle and Fähnle have found that the conversion factor varies between 12.6 T/μ_B for the Fe($12j$) site to 16.5 T/μ_B for the Fe($6g$) in Y_2Fe_{17}.[54]

The relative variation, in %, of $\langle B_{hf}\rangle$, $\langle \mu_{Fe}\rangle$ deduced from ND experiments, and M_s for $LuFe_{11.5}Ta_{0.5}$ as a function of the temperature are compared in Fig. 12.[4,6] For $LuFe_{11.5}Ta_{0.5}$,

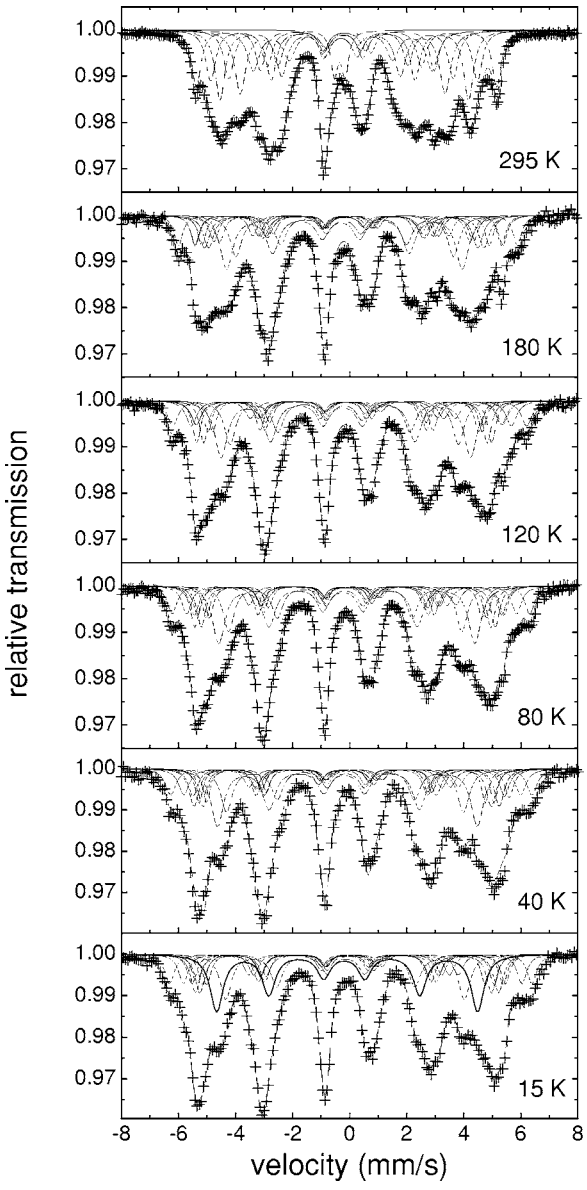

FIG. 8. The Mössbauer spectra of $DyFe_{11.5}Ta_{0.5}$ obtained at the indicated temperatures.

Fig. 12(a), all the parameters show a similar temperature dependence, although $\langle B_{hf}\rangle$ decreases faster when approaching room temperature. On the contrary, for $DyFe_{11.5}Ta_{0.5}$, Fig. 12(b), $\langle B_{hf}\rangle$ and $\langle \mu_{Fe}\rangle$ show different temperature dependence below and above of $T \approx T_{s2}$, indicating that the ratio between both magnitudes depends on the magnetic phase of the compound. In particular, $\langle f\rangle$ changes from 16.3 T/μ_B at $T < T_s$to 13.3 T/μ_B at $T > T_s$.

All these results clearly indicate that the approximation $B_{hf}(k) = f\mu_{Fe}(k)$ is an oversimplification of the real relationship between both magnitudes. A more accurate description of such relationship, which can also provide relevant information concerning the magnetic interactions that occur in this type of compounds, will be given in the following sections.

IV. LOCAL MODEL FOR THE MAGNETIC HYPERFINE FIELD

The most common expression for the hyperfine magnetic field experienced by the nucleus of an iron atom is[35,55]

$$B_{hf}(k) = B_c(k) + B_{orb}(k) + B_{dip}(k) = B_{cp}(k) + B_{4s}(k) + B_t(k) + B_{orb}(k) + B_{dip}(k) \quad (2)$$

where k represents the different crystallographic iron sites, $k = 8i$, $8j$, and $8f$, in the $ThMn_{12}$ structure.

The Fermi contact field, B_c, is isotropic and for transition metals is usually the main contribution to the total hyperfine field.[35,55] It is usually divided into three terms. The core polarization term, B_{cp}, represents the contribution from the spin density of the $1s$, $2s$, and $3s$ core electrons polarized by the $3d$ electrons of the parent atom. This term can be written as $B_{cp}(k) = \alpha\mu_{Fe}(k)$,[48,54,56,57] where $\mu_{Fe}(k)$ is the iron local magnetic moment at the k site, and α is the field at the nucleus produced by a $3d$ local iron moment of one μ_B. The $4s$ electrons, much more delocalized than the core electrons, can be polarized by the on site $3d$ magnetic moment and by the magnetic moments of the atoms in the first neighbor shell. The contribution coming from the $4s$ spin density polarized by the $3d$ electrons of the atom itself is the term B_{4s}, which is usually modeled as $B_{4s}(k) = \beta\mu_{Fe}(k)$,[56,57] where β mainly depends on the number of $4s$ spins contributing to the polarization and the intensity of the $4s$-$3d$ intra-atomic exchange interaction.[56,57] The field due to the $4s$ spin density polarized by the magnetic moments of the atoms in the first neighbor shell is the transferred hyperfine field, $B_t(k)$. This field shows contributions from both the NN iron and rare earth atoms:

$$B_t(k) = B_{tFe}(k) + B_{tR}(k). \quad (3)$$

In a mean field approximation, the iron sublattice transferred field, B_{tFe}, can be taken as proportional to the average magnetic moment of the iron atoms in the first neighbor shell, $\langle \mu_{Fe}\rangle_{1nn}(k)$.[56,57] A proportionality factor, $\zeta_{Fe}(k)$, different for each crystallographic site, should be included; this parameter depends on the number of $4s$ spins contributing to the polarization, the intensity of the inter-atomic exchange interactions $3d$-$4s$, and also on the particular magnetic and crystallographic environment of the involved atom.[57] Consequently, this term can be written as

$$B_{tFe}(k) = \zeta_{Fe}(k) Z_{Fe}(k) \langle \mu_{Fe}\rangle_{1nn}(k), \quad (4)$$

where $Z_{Fe}(k)$ is the number of iron NN; $Z_{Fe}(8i) = 12.4$, and $Z_{Fe}(8j) = Z_{Fe}(8f) = 9.5$, for $RFe_{11.5}Ta_{0.5}$.

The rare earth transferred field, B_{tR}, stems from the polarization of the iron $4s$ spin density by the R magnetic moments. However, the mechanism that transmits this polarization is not well established. It could be due to direct polarization of the conduction band, RKKY mechanism, or by means of the Campbell mechanism for the exchange interaction, where the $4f(R)$ spin moments polarize the $5d(R)$ ones, which are hybridized with the $3d$ electrons of iron.[27] The first mechanism has been invoked earlier by Li *et al.*[26] to explain the origin of B_{tR} in the $RFe_{11}Ti$ compounds,

TABLE V. Mössbauer hyperfine parameters for $DyFe_{11.5}Ta_{0.5}$. The symbol–indicates identical values for (I) and (II) sites.

Parameter	T, K	$8i_0$(I)	$8i_0$(II)	$8i_1$(I)	$8i_1$(II)	$8j_0$(I)	$8j_0$(II)	$8j_1$(I)	$8j_1$(II)	$8f_0$	$8f_1$	Total wt. aver.
B_{hf}, T	290	33.1	–	29.4	–	27.4	–	24.8	–	22.7	19.8	26.2
	180	37.0	33.6	33.5	31.4	30.5	29.4	28.0	27.8	25.7	23.9	29.1
	120	38.7	35.0	33.5	33.3	31.7	31.5	29.6	29.5	27.3	25.0	30.5
	80	39.1	36.0	33.8	33.3	32.3	32.1	30.1	30.3	27.9	25.5	31.1
	40	39.5	36.8	34.2	33.5	32.3	32.3	32.4	30.4	28.4	25.9	31.6
	15	39.5	36.8	34.0	33.5	32.5	32.4	32.3	30.5	28.5	26.1	31.7
δ,[a] mm/s	290	0.023	–	−0.072	–	−0.089	–	−0.150	–	−0.155	−0.158	−0.101
	180	0.109	–	0.052	–	−0.072	–	−0.060	–	−0.127	−0.074	−0.035
	120	0.174	–	0.103	–	−0.027	–	−0.024	–	−0.070	−0.076	0.008
	80	0.191	–	0.121	–	−0.019	–	−0.008	–	−0.048	−0.043	0.027
	40	0.219	–	0.140	–	0.008	–	0.011	–	−0.018	−0.030	0.050
	15	0.203	–	0.128	–	0.027	–	0.007	–	−0.020	−0.028	0.049
ε, mm/s	290	−0.015	–	−0.008	–	0.021	–	0.035	–	0.030	0.030	0.006
	180	−0.052	−0.012	0.016	−0.075	0.002	−0.036	−0.092	0.066	0.063	0.020	0.001
	120	−0.055	0.005	0.005	−0.010	−0.123	0.078	−0.081	0.066	0.055	0.003	0.002
	80	−0.028	−0.003	−0.022	−0.001	−0.101	0.092	−0.068	0.069	0.066	0.009	0.010
	40	−0.043	−0.009	−0.053	0.019	−0.137	0.160	−0.001	−0.020	0.056	−0.013	0.004
	15	−0.047	0.019	−0.044	0.000	−0.122	0.077	0.065	−0.015	0.050	−0.014	0.002

[a]Relative to α-iron at 295 K.

see Sec. V B. However, it is well known that the Campbell type exchange interaction is dominant in most R-Fe intermetallics, and explains satisfactorily their magnetic properties.

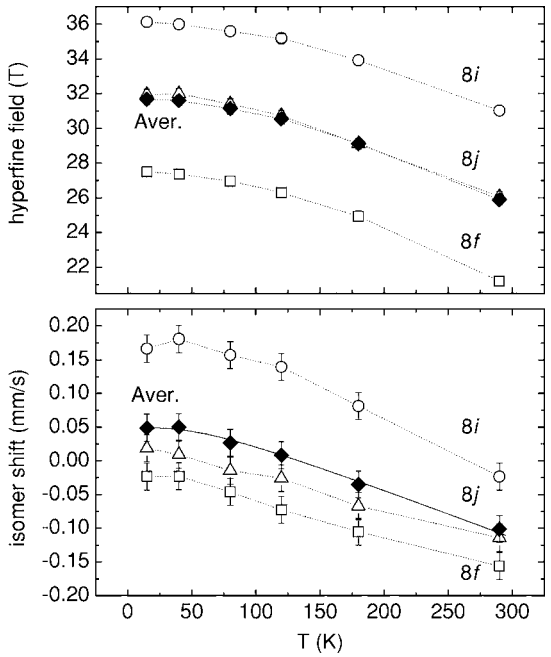

FIG. 9. Top panel: the temperature dependence of the three site weighted average hyperfine fields in $DyFe_{11.5}Ta_{0.5}$: $8i$ (○), $8j$ (△), and $8f$ (□) and the total average hyperfine field (♦). Bottom panel: the temperature dependence of the three site weighted average isomer shifts in $DyFe_{11.5}Ta_{0.5}$: $8i$ (○), $8j$ (△), and $8f$ (□) and the total average isomer shift (♦). The solid line through the total average isomer shift is the result of a fit with a Debye model of the second-order Doppler shift.

For this reason we have explored the possibility that B_{tR} stems from the polarization caused by the $4f(R)$ electrons in the $5d(R)$-$3d$(Fe) hybridized conduction band. According to this hypothesis, B_{tR} should be proportional to the R molecular field acting on the iron atoms

$$B_{tR}(k) = \zeta_R(k) Z_R(k) \gamma_R n_{RFe} \mu_R, \tag{5}$$

where $\zeta_R(k)$ is a proportionality factor which depends on the number of $4s$ spins contributing to the polarization, and also

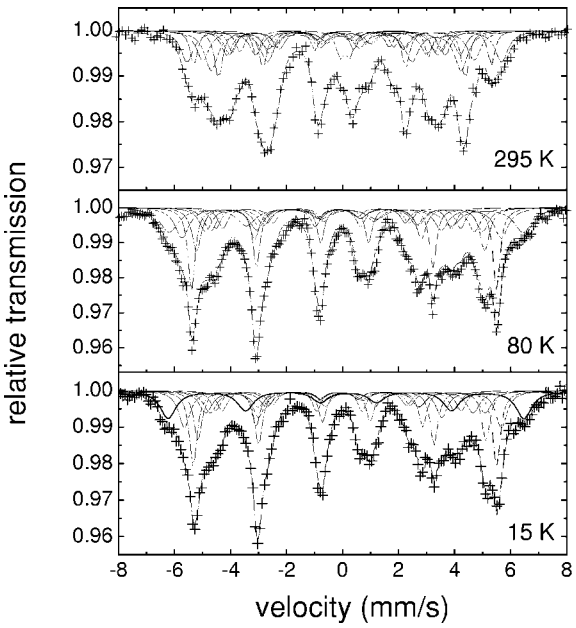

FIG. 10. The Mössbauer spectra of $TbFe_{11.5}Ta_{0.5}$ obtained at the indicated temperatures.

TABLE VI. Mössbauer hyperfine parameters for $TbFe_{11.5}Ta_{0.5}$. The symbol–indicates identical values for (I) and (II) sites.

Parameter	T,K	$8i_0$	$8i_1$	$8j_0$	$8j_1$	$8f_0$(I)	$8f_0$(II)	$8f_1$(I)	$8f_1$(II)	Total wt. aver.
B_{hf},T	290	35.0	30.2	27.8	27.4	26.0	24.0	23.3	21.7	27.9
	80	39.4	35.5	33.9	32.0	30.8	29.4	27.2	25.4	32.9
	15	39.6	35.3	33.7	32.0	31.1	29.3	27.3	25.8	32.9
δ,[a] mm/s	290	0.107	0.028	−0.163	−0.157	−0.107	–	−0.262	–	−0.094
	80	0.171	0.100	0.066	−0.114	−0.044	–	−0.152	–	0.008
	15	0.168	0.143	0.110	−0.067	−0.012	–	−0.130	–	0.039
ε, mm/s	290	−0.041	−0.173	−0.063	0.135	0.138	−0.076	0.066	0.082	−0.009
	80	−0.046	−0.131	−0.012	0.049	0.099	0.041	0.005	−0.036	−0.010
	15	−0.044	−0.130	−0.027	0.046	0.117	−0.021	−0.013	−0.019	−0.018

[a]Relative to α-iron at 295 K.

on the particular magnetic and crystallographic environment of the probe atom, $Z_R(k)=1$ is the number of rare earth NN, $\gamma_R=2(g_J-1)/g_J$, n_{RFe} is the R-Fe exchange coefficient,[58] and μ_R is the rare earth magnetic moment. The validity of this hypothesis will be checked in Sec. V B.

The remaining terms are the anisotropic contributions to the hyperfine field. The term B_{dip} is due to the dipolar interaction of the nuclear spin with the magnetic moments. It is usually described as the sum of a on-site contribution, B_{dip}(at), due to the aspherical valence electron density at the probe atom, and a lattice contribution, B_{dip}(latt), due to the moments of the neighboring atoms.[35,59] In R-Fe intermetallics the term B_{dip}(at) can only be calculated from band structure calculations, see, for instance, Ref. 59, while the lattice dipolar contribution can be obtained by performing a discrete lattice summation.[8,59] This term is small for R-Fe compounds,[26,48,54,59] and usually neglected, as we will discuss in Sec. V A for $RFe_{11.5}Ta_{0.5}$. B_{orb} is the magnetic field at the nucleus caused by the orbital motion of the unpaired electrons, $B_{orb}=2\mu_B\langle r^{-3}\rangle\langle L\rangle$.[35,55] In $3d$ metals this term may alternatively be expressed as

$$B_{orb} = g\mu_B\left\langle \frac{S(r)}{r^3}\right\rangle_{eff}\mu_{orb}, \tag{6}$$

where g is the Landé electronic factor, $\langle S(r)/r^3\rangle_{eff}$ is an average over all valence orbitals, which stems almost entirely from $3d$ orbitals in $3d$ transition metal atoms, and μ_{orb} is the iron orbital moment.[59] The electronic gyromagnetic g factor may have different values for parallel or perpendicular directions with respect to the site principal axis, which gives rise to the anisotropy of B_{orb}.[43] Grouping the anisotropic contributions in a single contribution, B_{anis}, the final expression for the hyperfine field at a given iron site, k, is

$$B_{hf}(k) = \alpha\mu_{Fe}(k) + \beta\mu_{Fe}(k) + \zeta_{Fe}(k)Z_{Fe}(k)\langle\mu_{Fe}\rangle_{1nn}(k) + \zeta_R(k)\gamma_R n_{RFe}\mu_R + B_{anis}(k). \tag{7}$$

The total hyperfine field at the nucleus is negative, i.e., opposite to the magnetization direction,[35,55] and its value strongly depends on the considered compound; for instance, it ranges between 20 and 40 T in $RFe_{12-x}M_x$. According to this convention, the term $B_{cp}=\alpha\mu_{Fe}(k)$ is also negative,[26,56,57] while the $B_{4s}=\beta\mu_{Fe}(k)$ term is positive;[26,56,57] the transferred field, B_t, can be either positive or negative.[26,56,57] Beuerle and Fähnle have reported, from *ab initio* calculations, that $B_{4s}+B_t$ is negative in Y_2Fe_{17}, which implies that B_t is negative in such a case.[54] The remaining terms B_{orb} and B_{dip} are positive and usually very much smaller than the isotropic contribution. Typical values of B_{anis} range between 1.4 and 2.8 T for intermetallic compounds.[11,26,42,43,48]

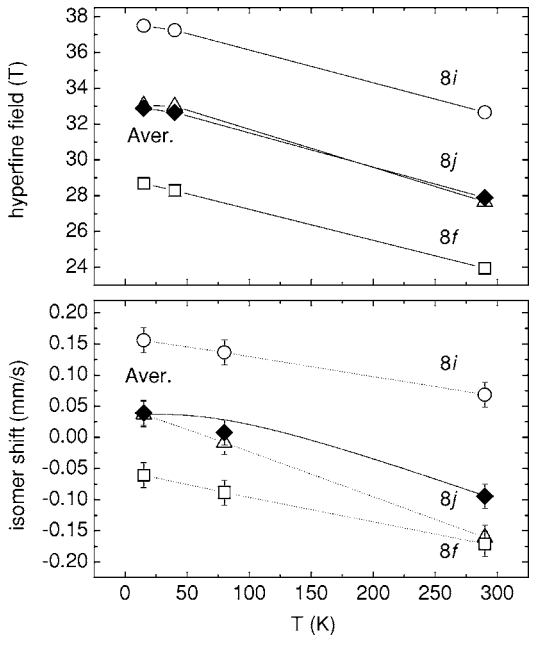

FIG. 11. Top panel: the temperature dependence of the three site weighted average hyperfine fields in $TbFe_{11.5}Ta_{0.5}$: $8i$ (○), $8j$ (△), and $8f$ (□) and the total average hyperfine field (◆). Bottom panel: the temperature dependence of the three site weighted average isomer shifts in $TbFe_{11.5}Ta_{0.5}$: $8i$ (○), $8j$ (△), and $8f$ (□) and the total average isomer shift (◆). The solid line through the total average isomer shift is the result of a fit with a Debye model of the second-order Doppler shift.

V. DETERMINATION OF THE CONTRIBUTIONS TO THE HYPERFINE FIELD

In this section Eq. (7) will be used to evaluate the different components of the iron hyperfine field. Our objectives

TABLE VII. Ratio between the hyperfine field and the iron magnetic moment of different $R\mathrm{Fe}_{12-x}M_x$ compounds at the indicated temperatures. $\langle f\rangle$ is the ratio calculated taking the average values $\langle B_{hf}\rangle$ and $\langle \mu_{Fe}\rangle$, and f_k are the ratios for the different crystallographic sites.

Compound	T, K	$f_{8i}(\mathrm{T}/\mu_B)$	$f_{8j}(\mathrm{T}/\mu_B)$	$f_{8f}(\mathrm{T}/\mu_B)$	$\langle f\rangle$ (T/μ_B)	Reference
$LuFe_{11.5}Ta_{0.5}$	15	14.3	15.4	15.0	14.9	This work
	290	13.7	14.4	14.3	14.1	This work
$DyFe_{11.5}Ta_{0.5}$	15	15.4	15.3	16.3	15.6	This work
	290	15.2	13.3	13.3	14.0	This work
$YFe_{11}Ti$	295	17.4	13.3	15.9	15.2	26
$HoFe_{11}Ti$	4.2	14.4	12.8	13.5	13.5	15
$YFe_{10}Si_2$	295	12.5	10.2	12.3	11.7	49 and 50
$YFe_{10}V_2$	4.2	15.1	13.3	13.1	13.8	51 and 52
$YFe_{10}Cr_2$	295				12.8	21
$YFe_{11.5}Mo_{0.5}$	295				15.1	53

are: first, to determine the relative values of $B_{cp}(k)$, $B_{4s}(k)$, and $B_{tFe}(k)$, which will provide a more accurate description of the relationship between $B_{hf}(k)$ and $\mu_{Fe}(k)$, and, second, to perform a careful analysis of the B_{tR} contribution in order to check the different proposed models for its origin. To this end the analysis of the hyperfine field data have been decoupled in two sections. Section V A is devoted to the nonmagnetic rare earth compound, $LuFe_{11.5}Ta_{0.5}$. Since in this case $B_{tR}=0$, and provided that enough simultaneous data of $B_{hf}(k)$ and $\mu_{Fe}(k)$ at different temperatures are available, the different contributions to $B_{hf}(k)$ are deduced from Eq. (7). In Sec. V B the rare earth contribution to B_{hf} is analyzed for $R\mathrm{Fe}_{11.5}\mathrm{Ta}_{0.5}$ and other R-Fe compounds.

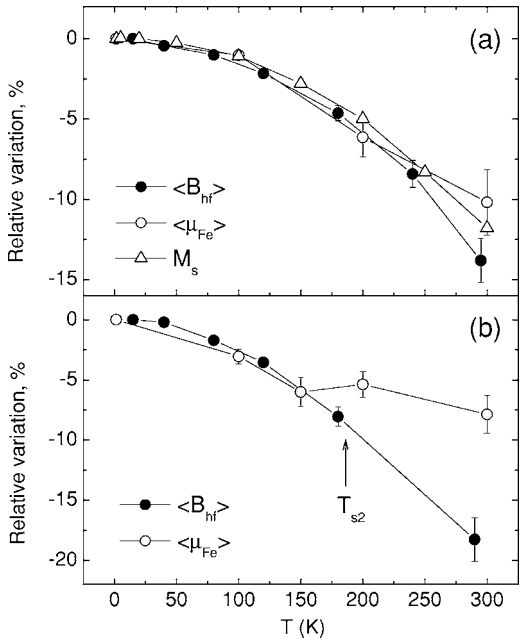

FIG. 12. Relative thermal variation, in %, of the total average hyperfine field, $\langle B_{hf}\rangle$, the iron magnetic moment obtained from ND experiments, $\langle \mu_{Fe}\rangle$, and the saturation magnetization, M_s, for $LuFe_{11.5}Ta_{0.5}$ (a) and $DyFe_{11.5}Ta_{0.5}$ (b).

A. Nonmagnetic rare earth case

Coehoorn *et al.* and Beuerle and Fähnle have found, from band structure calculations on Y-Fe compounds,[48,54] that the proportionality factor between the core polarization field, $B_{cp}(k)$, and the on-site magnetic moment, $\mu_{Fe}(k)$, is $\alpha=-11.3\ \mathrm{T}/\mu_B$, independently of the site type. A similar proportionally factor, $-10\ \mathrm{T}/\mu_B$, has been found for $3d$ impurities in nickel.[57] These results seem to indicate that the polarization of the core shells by the on site $3d$ moment is little sensitive to the environment of the iron atom. Hence, we will take $\alpha=-11.3\ \mathrm{T}/\mu_B$ for $LuFe_{11.5}Ta_{0.5}$ by similarity with the Y-Fe compounds.[48,54]

There are very few reports on the values of B_{dip}(at) and B_{dip}(latt) for intermetallic compounds, because this term is usually neglected.[26,48,54,59] Coehoorn has calculated these values for YFe_2, obtaining B_{dip}(at)=0.3 and −0.1 T, and B_{dip}(latt)=0.6 and −0.2 T for the two magnetically distinct sites.[59] The calculation of B_{dip}(at) in our compounds is beyond of the scope of this work, but we have calculated the B_{dip}(latt) term for $LuFe_{11.5}Ta_{0.5}$ in order to check if B_{dip} can be neglected in our analysis. In the calculation of B_{dip}(latt) the magnetic moments at the iron $8i$, $8j$, $8f$ sites and at the rare earth $2a$ site have been taken from our previous ND study.[6] In order to account for the random substitution of tantalum, the $8i$ sites are considered to be occupied only by iron atoms with an average magnetic moment corresponding to a substitution concentration of 0.5/4. The calculation was extended for atoms in a sphere of increasing radius, and convergence was attained within 1% for radius of about 50 Å. The B_{dip}(latt) calculated for a coordination radius of 100 Å are collected in Table IX. They vary in value and sign at each site, but in all cases they are lower than 1% of the total hyperfine field. Assuming that the B_{dip}(at) term is similar to those obtained for YFe_2, the total dipolar field is of the order of the experimental error in B_{hf}, therefore, we can conclude that the neglect of B_{dip} is a good approximation in the analysis of our compounds.

According to Eq. (6), the orbital field can be expressed as $B_{orb}=A\mu_{orb}$.[59] Consequently, if μ_{orb} and the conversion factor A are known it is possible to estimate B_{orb} in

TABLE VIII. $\zeta_{Fe}(k)$ parameters in different $R\mathrm{Fe}_{12-x}M_x$, $x \leqslant 1$, compounds (see details in the text).

Compound	β	$\zeta_{Fe}(8i)$	$\zeta_{Fe}(8j)$	$\zeta_{Fe}(8f)$	Reference
$\mathrm{LuFe}_{11.5}\mathrm{Ta}_{0.5}$	3.7	−0.69	−0.87	−0.71	this work
$\mathrm{YFe}_{11.5}\mathrm{Mo}_{0.5}$	3.7	−0.58	−0.84	−0.62	24 and 66
$\mathrm{YFe}_{11}\mathrm{Ti}$	3.7	−0.78	−0.99	−0.90	26

$\mathrm{LuFe}_{11.5}\mathrm{Ta}_{0.5}$. Up to our knowledge, there are no direct determinations of μ_{orb} on the $R\mathrm{Fe}_{12-x}M_x$ series, except for $\mathrm{ErMn}_3\mathrm{Fe}_9$. In this compound, it has been derived, from x-ray magnetic circular dichroism, XMCD, measurements, that $\mu_{orb}=0.12\mu_B$.[60] A very similar value, $\mu_{orb}=0.1\ \mu_B$ has been found, also from XMCD measurements, in $\mathrm{Nd}_2\mathrm{Fe}_{14}\mathrm{B}$,[61] a highly magnetically anisotropic compound with iron only standing for the $3d$ transition metal NN. Our best estimation for $R\mathrm{Fe}_{11.5}\mathrm{Ta}_{0.5}$ is, therefore, $\mu_{orb}=0.11\pm0.01\ \mu_B$. The conversion factor, see Eq. (6), depends on the type of atom and on the details of the electronic structure. According to Coehoorn,[59] it depends only on the type of atom, hence, it could be evaluated as the ratio of B_{orb} and μ_{orb} of α iron. Moreover, this relation is expected to hold irrespectively of the symmetry of the site since the incompletely quenched orbital moment in Fe has been proven to be related to the hybridization of the Fe atom with the host and the occupation of the iron $3d$ states.[62] The orbital conversion factor, A, has been evaluated for α-Fe from fully relativistic calculations of the magnetic orbital moment and hyperfine field contributions,[63] yielding $A=42\ \mathrm{T}/\mu_B$, which applied to our estimation of $\mu_{orb}=0.11\mu_B$ gives $B_{orb}=4.6$ T for $\mathrm{LuFe}_{11.5}\mathrm{Ta}_{0.5}$. However, this conversion factor was determined from calculations that gave a very poor prediction of B_{hf} and μ_{orb}, the latter being almost 50% too low, so $B_{orb}=4.6$ T is overestimated. A more naïve approach is to obtain the ratio between the experimentally determined values of $B_{hf}=33.9$ T,[64] and $\mu_{Fe}=2.07\mu_B$, determined from XMCD measurements,[65] of α-iron, $A=16.5\ \mathrm{T}/\mu_B$, and assume that it may be directly applicable to the orbital moments to determine B_{orb}. Applied to our estimation of μ_{orb}, we get $B_{orb}=1.8$ T. As a conclusion of these arguments, B_{orb} for $\mathrm{LuFe}_{11.5}\mathrm{Ta}_{0.5}$ may have values in the range $1.8<B_{orb}<4.6$ T, the actual value being probably intermediate. In fact the value $B_{orb}=2.8$ T has been proposed earlier for $R\mathrm{Fe}_{11}\mathrm{Ti}$;[26] hence, in what follows we assign $B_{anis}=B_{orb}=2.8$ T, which corresponds to $A=25\ \mathrm{T}/\mu_B$. Since B_{anis} is a small contribution to the total hyperfine field this approximation is not expected to significantly affect the determination of the components of $B_{hf}(k)$, as we discuss below.

Summarizing, we can write Eq. (7) in the following way:

$$B_{hf}(k) = -11.3\mu_{Fe}(k) + \beta\mu_{Fe}(k) + \zeta_{Fe}(k)Z_{Fe}(k)\langle\mu_{Fe}\rangle_{1nn}(k) + 2.8. \quad (8)$$

The magnetic moments $\mu_{Fe}(k)$ at $T=1.5$, 100, 200, and 300 K are known from our previous ND experiments.[6] Interpolating the present $B_{hf}(k)$ values at those temperatures one obtains from Eq. (8) a set of twelve equations with four unknown quantities. A least square fit of these equations gives the β and $\zeta_{Fe}(k)$ coefficients displayed in Table VIII. With these values, $B_{4s}(k)$ and $B_t(k)$ are derived. They are collected in Table IX together with the values of $B_{cp}(k)$, $\mu_{Fe}(k)$, and the experimental and calculated values of $B_{hf}(k)$ at $T=15$ K. The different components of $B_{hf}(k)$ agree with the results found by Li *et al.* for $\mathrm{YFe}_{11}\mathrm{Ti}$,[26] although these authors used a unique value of $\zeta_{Fe}(k)$. They are also consistent with the calculated values of $B_{4s}+B_t$ for $\mathrm{Y}_2\mathrm{Fe}_{17}$,[54] and with the calculated values of B_{cp} and B_{4s} of iron impurities in nickel.[57]

The hyperfine field contains a term, $[B_{cp}(k)+B_{4s}(k)]$, which is proportional to the on-site magnetic moment $\mu_{Fe}(k)$, and a term, $[B_{tFe}(k)+B_{anis}]$, which is not proportional to it. The ratio $f=B_{hf}(k)/\mu_{Fe}(k)$ will be site independent whenever $[B_{cp}(k)+B_{4s}(k)] \gg [B_{tFe}(k)+B_{anis}]$, or when $\zeta_{Fe}(k)Z_{Fe}(k)$ and $\mu_{Fe}(k)$ have similar values at the different iron sites. However, as shown in Table IX, the transferred hyperfine fields are similar to the $[B_{cp}(k)+B_{4s}(k)]$ term. Moreover, $B_{tFe}(k)$ is different at each iron site. Consequently, the observed scattering of the values of f_k can be interpreted as due to the influence of the $B_{tFe}(k)$ term, that is, to the fact that the interaction of the $4s$ valence electrons with the NN iron atoms is different at each crystallographic site.

To test the model further, the same procedure was applied to other $R\mathrm{Fe}_{12-x}M_x$. Unfortunately, we have not found $\mu_{Fe}(k)$ and $B_{hf}(k)$ data at different temperatures for the same $R\mathrm{Fe}_{12-x}M_x$, with $R=$ nonmagnetic rare earth. Since experi-

TABLE IX. The lattice dipolar hyperfine field, the iron magnetic moments, and the different contributions to the hyperfine field of $\mathrm{LuFe}_{11.5}\mathrm{Ta}_{0.5}$ at $T=15$ K (see details in the text).

Site	$B_{dip}(latt)$ (T)	$\mu_{Fe}(\mu_B)$	B_{cp}(T)	B_{4s}(T)	B_{tFe}(T)	B_{anis}(T)	B_{hf}(T) cal	$\langle B_{hf}\rangle$(T) exp
$8i$	0.08	2.34	−26.4	10.0	−19.9	2.8	−33.5	−33.6
$8j$	−0.22	1.95	−22.1	8.4	−19.2	2.8	−30.1	−30.1
$8f$	0.17	1.74	−19.6	7.5	−16.6	2.8	−26.0	−26.0
Total wt. aver.	0.01	1.99	−22.5	8.6	−18.5	2.8	−29.7	−29.7

mental values of $\mu_{Fe}(k)$ and $B_{hf}(k)$ are available for just one temperature, only one set of three equations is given by Eq. (8). In order to solve for β, $\zeta_{Fe}(8i)$, $\zeta_{Fe}(8j)$, and $\zeta_{Fe}(8f)$ we will take $\beta=3.7$ T/μ_B, as obtained for $R\mathrm{Fe}_{11.5}\mathrm{Ta}_{0.5}$, and the study will be restricted to similar compositions, that is, $R\mathrm{Fe}_{12-x}M_x$ compounds with $x\leqslant 1$.[24,26,66] The $\zeta_{Fe}(k)$ parameters obtained with this procedure are displayed in Table VIII. For all the studied compounds the largest coefficient is $\zeta_{Fe}(8j)$. We have checked that this conclusion is neither affected by the particular value of β nor by that of B_{anis}. According to the proposed expression for the iron transferred field, Eq. (4), $B_{tFe}(k)$ depends, through the $\zeta_{Fe}(k)$ coefficients, on the number of the 4*s* spins contributing to the polarization and the intensity of the interatomic 3*d*-4*s* exchange interaction. Consequently, this hierarchy in $\zeta_{Fe}(k)$ suggests that, in the $R\mathrm{Fe}_{12-x}M_x$ compounds with $x\leqslant 1$, the exchange interaction of the 4*s* valence electrons with the 3*d* electrons of the NN atoms is stronger at the 8*j* site. This can be explained in terms of the crystallographic and magnetic environments of the different iron sites. The 8*j* site has four 8*f* NN iron atoms at ~2.4 Å, whereas the 8*i* site has four 8*f* NN iron atoms at ~2.6 Å, and the 8*f* sites has just two 8*f* NN atoms at ~2.4 Å,[6] i.e., the iron atoms located at the 8*j* site have both the largest number of 8*f* NN and the smallest average Fe-Fe distances to them. Taking into account that the 3*d* electrons are more delocalized in the 8*f* iron sites,[6] the particular NN environment of the 8*j* site could explain why the 4*s*-3*d* exchange interaction is stronger at the 8*j* site.

Finally, it should be noted that Eq. (7) can also be used to get a deeper insight in the relationship between the average values of the hyperfine field and the iron magnetic moment. Taking averages on both sides of Eq. (7), one obtains

$$\langle B_{hf}\rangle = \{-11.3 + \langle\beta\rangle + \langle\zeta_{Fe}\rangle\}\langle\mu_{Fe}\rangle + \langle\zeta_R\rangle\gamma_R n_{RFe}\mu_R + \langle B_{anis}\rangle = \langle B_{cFe}\rangle + \langle B_{tR}\rangle + \langle B_{anis}\rangle, \quad (9)$$

where $\langle B_{cFe}\rangle$ is the part of the Fermi contact field which depends exclusively on the iron sublattice. For the nonmagnetic rare earth compounds, $\mu_R=0$, this expression implies that $\langle B_{hf}\rangle \sim \langle f\rangle\langle\mu_{Fe}\rangle$, whenever $\langle B_{anis}\rangle \ll \langle B_{cFe}\rangle$. However, the parameter $\langle f\rangle$ which relates $\langle B_{hf}\rangle$ and $\langle\mu_{Fe}\rangle$ depends on the number of 4*s* spins contributing to the polarization and on the intensity of the intra and inter-atomic exchange interactions. Consequently, the parameter $\langle f\rangle$ will differ from one type of compound to another, and it reflects the modifications induced in the conduction electron density of states by different substitutions or dilutions, or in nitrogen and hydrogen derivatives.[26,67]

B. Magnetic rare earth case

In $R\mathrm{Fe}_{11.5}\mathrm{Ta}_{0.5}$ there is a clear influence of the rare earth in the average iron hyperfine field, as observed in Fig. 13, where $\langle B_{hf}\rangle$ is shown as a function of the atomic number of the rare earth at different temperatures. The average hyperfine field decreases in the sequence Tb to Lu, being less pronounced the difference at $T=295$ K. The maximum difference is 3.2 and 2.4 T at 15 K and 295 K, respectively. The increase in $\langle B_{hf}\rangle$ when Lu is substituted by a magnetic rare earth atom has also been observed in other intermetallic compounds when substituting Lu or Y by either light or heavy rare earth.[14–19,21,30,31,68–74]

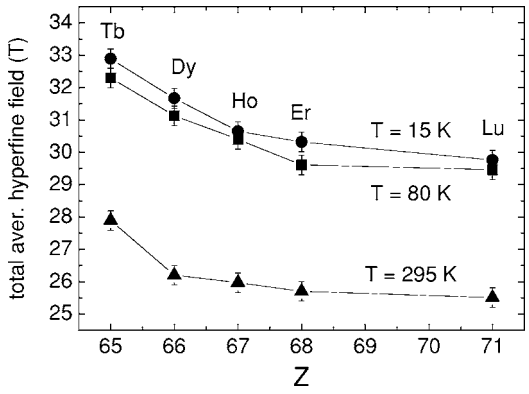

FIG. 13. The total average hyperfine field, $\langle B_{hf}\rangle$, as a function of the atomic number of the rare earth at $T=15$ (•), 80 (■), and 295 K (▲).

To a first approximation, the rare earth contribution to $\langle B_{hf}\rangle$ may be analyzed in terms of a two sublattice model. According to this model, the total hyperfine field can be written as

$$\langle B_{hf}\rangle = \langle B_{Fe}\rangle + \langle B_{tR}\rangle = \langle B_{Fe}\rangle + \langle\zeta_R\rangle\gamma_R n_{RFe}\mu_R, \quad (10)$$

where $\langle B_{Fe}\rangle$ represents the contribution coming from the iron sublattice, and B_{tR}, as given by Eq. (5), represents the contribution coming from the rare earth sublattice. Within this model the $\langle B_{Fe}\rangle$ term is assumed to be the same for all the members of a given series and should be taken as the value of $\langle B_{hf}\rangle$ for $\mathrm{LuFe}_{11.5}\mathrm{Ta}_{0.5}$. However, some cautions are necessary when applying this approach. According to Eq. (9), the total average hyperfine field of $\mathrm{LuFe}_{11.5}\mathrm{Ta}_{0.5}$ is made up by two components, $\langle B_{cFe}\rangle$ and $\langle B_{anis}\rangle$, where $\langle B_{anis}\rangle$ is the sum of $\langle B_{dip}\rangle$ and $\langle B_{orb}\rangle$. It has been observed in $\mathrm{Nd}_2\mathrm{Fe}_{14}\mathrm{B}$ that μ_{orb}changes at the SRT, from $\mu_{orb}=0.1\mu_B$ in the axial magnetic phase to $0.05\mu_B$ in the canted magnetic phase.[61] Such a change would bear a reduction of $\langle B_{anis}\rangle$ from 2.5 to 1.2 T when passing from the axial to the canted magnetic phase, under the assumption of $A=25$ T/μ_B. Moreover, we have observed in $\mathrm{DyFe}_{11.5}\mathrm{Ta}_{0.5}$, see Fig. 12(b), that the ratio between $\langle B_{hf}\rangle$ and $\langle\mu_{Fe}\rangle$ changes at the SRT. Consequently, one can expect that the value of $\langle B_{anis}\rangle$ and, hence, of $\langle B_{Fe}\rangle$, of a given $R\mathrm{Fe}_{11.5}\mathrm{Ta}_{0.5}$ can be different than those of the $\mathrm{LuFe}_{11.5}\mathrm{Ta}_{0.5}$ when the compound is not magnetically axial. For that reason, we have restricted the use of the two sublattice model to those cases in which magnetic and nonmagnetic rare earth compounds have the same macroscopic EMD. We have checked that the differences in $\langle B_{dip}\rangle$ can be neglected in such a case. For instance, B_{dip}(latt)=0.19, −0.36, 0.24 T for the 8*i*, 8*j*, and 8*f* sites of $\mathrm{ErFe}_{11.5}\mathrm{Ta}_{0.5}$, which gives an average value of 0.02 T, very similar to those found for $\mathrm{LuFe}_{11.5}\mathrm{Ta}_{0.5}$, see Table IX.

In Fig. 14(a) $\langle B_{hf}\rangle$ is plotted as a function of the product $\gamma_R n_{RFe}\mu_R$ at $T=15$ and 295 K for the $R\mathrm{Fe}_{11.5}\mathrm{Ta}_{0.5}$ magnetically axial compounds. The values of the exchange param-

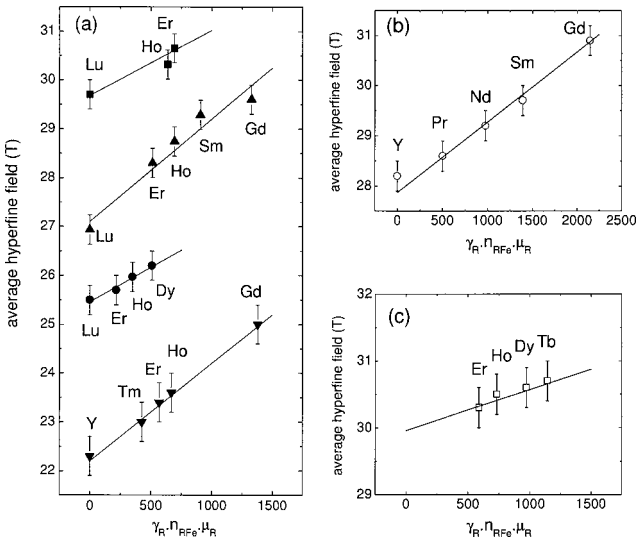

FIG. 14. (a) The total average hyperfine field, $\langle B_{hf}\rangle$, as a function of the product $\gamma_R n_{RFe}\mu_R$ for $R\mathrm{Fe}_{11.5}\mathrm{Ta}_{0.5}$ at $T=15$ K (■), $R\mathrm{Fe}_{11.5}\mathrm{Ta}_{0.5}$ at $T=295$ K (•), $R\mathrm{Fe}_{11}\mathrm{Ti}$ at $T=4.2$ K (▲), and $R\mathrm{Fe}_{10}\mathrm{Cr}_2$ at $T=78$ K (▲). (b) The total average hyperfine field, $\langle B_{hf}\rangle$, as a function of the product $\gamma_R n_{RFe}\mu_R$ for rhombohedral $R_2\mathrm{Fe}_{17}$ at $T=85$ K. (c) The total average hyperfine field, $\langle B_{hf}\rangle$, as a function of the product $\gamma_R n_{RFe}\mu_R$ for hexagonal $R_2\mathrm{Fe}_{17}$ at $T=85$ K.

eters, n_{RFe}, and μ_R have been taken from Refs. 75 and 6, respectively. At $T=15$ K the value of $\langle B_{hf}\rangle$ for $\mathrm{ErFe}_{11.5}\mathrm{Ta}_{0.5}$ has also been included because it is in a canted phase with a small canting angle, $\theta_c=25°$. In both cases, 15 and 295 K, the experimental data have been fit with the linear expression given by Eq. (10). The fit gives the same $\langle\zeta_R\rangle$ values for both temperatures, and values of $\langle B_{Fe}\rangle$which coincide with those of $\langle B_{hf}\rangle$ for $\mathrm{LuFe}_{11.5}\mathrm{Ta}_{0.5}$ at those temperatures, see Table X. This result proves the adequacy of both the two sublattice model and the proportionality of B_{tR} with $\gamma_R n_{RFe}\mu_R$. Moreover, this allows us to understand the behavior of $\langle B_{hf}\rangle$ shown in Fig. 13 as due to the $\langle B_{tR}\rangle$ term: when Z is decreased (that is, in the trend Er to Tb in Fig. 13), γ_R, and consequently $\langle B_{tR}\rangle$, increase, and as a result $\langle B_{hf}\rangle$ increase from Er to Tb.

The validity of the hypothesis of a linear dependence of B_{tR} with $\gamma_R n_{RFe}\mu_R$ can be extended analyzing different series of intermetallic compounds, $R\mathrm{Fe}_{12-x}M_x$, $R_2\mathrm{Fe}_{17}$, and $R_2\mathrm{Fe}_{14}\mathrm{B}$, wherever $\langle B_{hf}\rangle$ data are available. For each series the R magnetic moment is considered as $\mu_R=g_J J_R[1-(T/T_c)^n]=\kappa(T)g_J J_R$. Since T_c varies at most 10% within a lanthanide series $\kappa(T)$ is taken as a constant that is implicit in ζ_R; at any rate, $\kappa(T)=1$ for $T=15$ K and between 0.7 and 0.8 for $T=295$ K. Briefly, the approximation $B_{tR}=\zeta_R(T)\gamma_R n_{RFe} g_J J_R$ has been used in the analysis of other series different than $R\mathrm{Fe}_{11.5}\mathrm{Ta}_{0.5}$. In all cases only those compounds in which the EMD is identical, either axial or planar, to that of the nonmagnetic R reference compound have been considered. In general, the R-Fe compounds considered are magnetically axial, except the $R_2\mathrm{Fe}_{17}$ which are all planar. The values of n_{RFe} have been calculated from T_c using the mean field expression.[75] The experimental values of $\langle B_{hf}\rangle$, T_c and cell volume have been taken from the references mentioned in Table X.

The $\langle B_{hf}\rangle$ values as a function of the product $\gamma_R n_{RFe}\mu_R$ for other series different than $R\mathrm{Fe}_{11.5}\mathrm{Ta}_{0.5}$ are depicted in Figs. 14 and 15 (left panels), and show in all cases a clear linear dependence. The $\langle B_{Fe}\rangle$and ζ_R fit parameters are collected in Table X. In all the series the value of $\langle B_{Fe}\rangle$ obtained from the extrapolation of the linear fit to $\mu_R=0$ agrees well with the value for the nonmagnetic rare earth isostructural compound, see Table X. For the hexagonal $R_2\mathrm{Fe}_{17}$ this check was not possible since there are no data for $\mathrm{Lu}_2\mathrm{Fe}_{17}$. It can be observed that the values of the ζ_R are similar, although they depend on the particular series, as could be expected from a

TABLE X. $\langle\zeta_R\rangle$ and $\langle B_{Fe}\rangle$ parameters in different $R\mathrm{Fe}_{12-x}M_x$ compounds. The values of $\langle B_{hf}\rangle$ has been included for comparison (see details in the text).

Compound	T(K)	$\langle\zeta_R\rangle$ (T/μ_B)	$\langle B_{Fe}\rangle$(T)	$\langle B_{hf}\rangle$	Reference
$R\mathrm{Fe}_{11.5}\mathrm{Ta}_{0.5}$	15	0.014(5)	29.7(3)		This work
$\mathrm{LuFe}_{11.5}\mathrm{Ta}_{0.5}$	15			29.7(3)	This work
$R\mathrm{Fe}_{11.5}\mathrm{Ta}_{0.5}$	295	0.014(5)	25.4(3)		This work
$\mathrm{LuFe}_{11.5}\mathrm{Ta}_{0.5}$	295			25.5(3)	This work
$R\mathrm{Fe}_{11}\mathrm{Ti}$	4.2	0.021(6)	27.1(3)		14–16 and 30
$\mathrm{LuFe}_{11}\mathrm{Ti}$	4.2			27.0(3)	31
$R\mathrm{Fe}_{11}\mathrm{Ti}$	295	0.029(6)	22.7(3)		14–16, 19, and 30
$\mathrm{LuFe}_{11}\mathrm{Ti}$	295			22.9(3)	31
$R\mathrm{Fe}_{10}\mathrm{Cr}_2$	78	0.020(6)	22.2(3)		21 and 75
$\mathrm{YFe}_{10}\mathrm{Cr}_2$	78			22.3(3)	21
$R_2\mathrm{Fe}_{14}\mathrm{B}$	295	0.023(7)	28.2(6)		73
$\mathrm{YFe}_{14}\mathrm{B}$	295			28.4(3)	73, 74, and 76
$R_2\mathrm{Fe}_{17}$ (rhomb)	85	0.014(4)	27.8(3)		68 and 69
YFe_{17} (rhomb)	85			28.2(3)	79
$R_2\mathrm{Fe}_{17}$ (hex)	85	0.010(6)	29.9(3)		70–72, 77, and 78

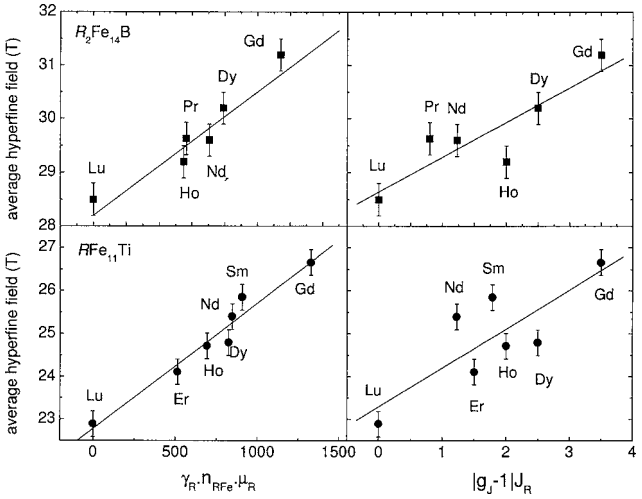

FIG. 15. Left panel: The total average hyperfine field, $\langle B_{hf}\rangle$, as a function of the product $\gamma_R n_{RFe}\mu_R$ for $R_2Fe_{14}B$ at $T=295$ K (■), and $RFe_{11}Ti$ at $T=295$ K (•). Right panel: The total average hyperfine field, $\langle B_{hf}\rangle$, as a function of the product $|g_J-1|J_R$ for $R_2Fe_{14}B$ at $T=295$ K (■), and $RFe_{11}Ti$ at $T=295$ K (•).

model where all the details of the surrounding crystallography are encompassed by the fit constant.

Assuming that the interaction mechanism is of the RKKY type, Li *et al.*[26] proposed earlier that B_{tR} should be proportional to $(g_J-1)J_R$ (actually, they use the absolute value $|g_J-1|J_R$ in their Fig. 5), being the proportionality factor a constant for a given series of isostructural compounds. In order to compare both models, the most recent and accurate $R_2Fe_{14}B$ and $RFe_{11}Ti$ data available are plotted in Fig. 15 as a function of $\gamma_R n_{RFe}\mu_R$ (left panels) and $|g_J\text{-}1|J_R$ (right panels). As one can observe from this figure the data points coalesce with little scatter into a linear dependence of $\gamma_R n_{RFe}\mu_R$, see left panel of Fig. 15. On the contrary, the scatter is very significant, specially for the light rare earth compounds, when $\langle B_{hf}\rangle$ is plotted against $|g_J\text{-}1|J_R$, see right panel of Fig. 15. Of course, the main differences between both models originate from the n_{RFe} coefficient. This factor is nearly constant for heavy rare earths, and, consequently, in such a case, the predictions of both models are very similar. However, n_{RFe} increases strongly in the light rare earth compounds, which has the effect of shifting the points to the common linear dependence of the heavy rare earth compounds.

Consequently, it can be concluded that B_{tR} is mainly due to the $4f(R)$-$3d$(Fe) exchange interaction via the $3d$(Fe) -$5d(R)$ hybridized band, rather than by the RKKY mechanism.

Finally, the proposed expression for $\langle B_{hf}\rangle$ is used to determine the decrease of the anisotropy component, ΔB_{anis}, in the magnetically non axial compounds. $\langle B_{hf}\rangle$ can be written as

$$\langle B_{hf}\rangle = \langle B_{hf}\rangle(\mathrm{LuFe_{11.5}Ta_{0.5}}) + \Delta\langle B_{anis}\rangle + \langle\zeta_R\rangle\gamma_R n_{RFe}\mu_R. \quad (11)$$

Provided that $\langle B_{hf}\rangle(\mathrm{LuFe_{11.5}Ta_{0.5}})$ and μ_R are known at different temperatures, and $\langle\zeta_R\rangle=0.0014$ T/μ_B in $R\mathrm{Fe_{11.5}Ta_{0.5}}$, one can easily determine the value of $\Delta\langle B_{anis}\rangle$ for $\mathrm{DyFe_{11.5}Ta_{0.5}}$ at $T<295$ K, and for $\mathrm{TbFe_{11.5}Ta_{0.5}}$ in the whole measured temperature range. These values are independent of the temperature and amount to 0.5 and 1.4 T for $\mathrm{DyFe_{11.5}Ta_{0.5}}$ and $\mathrm{TbFe_{11.5}Ta_{0.5}}$, respectively, very similar to the variation of B_{anis} observed in $Nd_2Fe_{14}B$.[61] At present we do not have a reasonable explanation for the greater value of $\Delta\langle B_{anis}\rangle$ obtained for the Tb compound, but this result is in agreement with the fact that the differences between B_{hf}(I) and B_{hf}(II) are also larger in the Tb compound.

VI. CONCLUSIONS

The Mössbauer spectra of $R\mathrm{Fe_{11.5}Ta_{0.5}}$, R =Tb, Dy, Ho, Er, and Lu, have been analyzed with a model that considers both the distribution of the tantalum atoms in the NN environment of an iron atom and the relative orientation of B_{hf} and V_{zz}. The different directions of V_{zz} in the three inequivalent iron sites of the $ThMn_{12}$ structure have been determined from a close examination of the point symmetry of each iron site.

The obtained hyperfine parameters, as well as their changes per tantalum NN, are similar to those obtained for $R\mathrm{Fe_{11}Ti}$, although in the analysis of the Mössbauer spectra of $R\mathrm{Fe_{11.5}Ta_{0.5}}$ it was not necessary to assume a linear dependence of the hyperfine parameters upon the number of tantalum NN.

The Mössbauer spectral investigations are consistent with the previous magnetic measurements and give information about the EMD in the basal plane for the magnetically nonaxial compounds. The Mössbauer spectra of $\mathrm{ErFe_{11.5}Ta_{0.5}}$ at $T<T_s$ indicate that the EMD is contained in the (100) plane of the tetragonal unit cell. For $\mathrm{DyFe_{11.5}Ta_{0.5}}$ the Mössbauer spectra at $T<T_{s2}$ are consistent with the iron moments aligned along the [100] direction of the basal plane. Finally, the analysis of $\mathrm{TbFe_{11.5}Ta_{0.5}}$ data is consistent with the iron magnetic moments aligned parallel to the [110] direction within the basal plane of the tetragonal unit cell.

The ratio f_k between the site weighted average hyperfine fields $B_{hf}(k)$ and the local magnetic moments, $\mu_{Fe}(k)$, has been calculated in order to revise critically the constant conversion factor approximation which relate magnetic moments and hyperfine fields. From our analysis for $R\mathrm{Fe_{11.5}Ta_{0.5}}$ and other $R\mathrm{Fe_{12-x}}M_x$ it is shown that f_k can be significatively different at each crystallographic iron site. It is also shown that the ratio between the average values of B_{hf} and μ_{Fe} can be different depending on the compound, and on the magnetic state of a given compound.

A local model for the hyperfine field has been developed, which allows to take into account the different contributions to the hyperfine field per site, and to treat separately the iron and rare earth contributions. Within this framework, the rare earth transferred field, B_{tR}, has been considered to be proportional to the R-Fe exchange interaction generated by the rare earth nn of the iron moments, presuming that the rare earth magnetic polarization propagates via the $5d(R)$-$3d$(Fe) hybridized band, according to the Campbell mechanism.

The analysis of the iron and rare earth contributions to B_{hf} has been decoupled by treating separately the nonmagnetic

and magnetic rare earth compounds. Applying of the model to $LuFe_{11.5}Ta_{0.5}$, i.e., in a compound with nonmagnetic rare earth, the contributions to $B_{hf}(k)$ originating exclusively from the iron sublattice were deduced. The main conclusions were: the iron transferred fields, $B_{tFe}(k)$, are different at each crystallographic site, and they have similar values to the sum of $B_{cp}(k)$ and $B_{4s}(k)$, the contributions which are proportional to $\mu_{Fe}(k)$. Therefore, $B_{hf}(k)$, which is the sum of all three terms, cannot fulfill the simple rule of $B_{hf}(k)/\mu_{Fe}(k)=$const. A similar analysis of $B_{hf}(k)$ has been done for other $R\mathrm{Fe}_{12-x}M_x$, where R is nonmagnetic, confirming the lack of this proportionality at the local site level. Common trends have been found in the relative values of the $B_{tFe}(k)$ terms, which can be understood in terms of the particular magnetic and crystallographic environment of each iron site. Additionally, the lattice dipolar hyperfine field has been calculated for $LuFe_{11.5}Ta_{0.5}$,and it is shown the neglecting B_{dip} is a right procedure in the analysis of our compounds.

The analysis of the magnetic rare earth $R\mathrm{Fe}_{11.5}\mathrm{Ta}_{0.5}$ allows to determine the origin of the B_{tR} term. The total hyperfine field is treated as the sum of the iron and rare earth contributions, in the framework of a two sublattice model, for the magnetically axial $R\mathrm{Fe}_{11.5}\mathrm{Ta}_{0.5}$. This approach is not applicable to the magnetically nonaxial phases because the values of the anisotropic contribution to B_{hf} can considerably affect the determination of B_{tR}. A linear dependence of B_{tR} with the product $\gamma_R n_{RFe}\mu_R$ has been found, indicating that this term is mainly originated from the indirect $4f(R)$ -$3d$(Fe) exchange interaction. The same analysis of the B_{tR} term has been performed on other $R\mathrm{Fe}_{12-x}M_x$, $R_2\mathrm{Fe}_{14}\mathrm{B}$, and $R_2\mathrm{Fe}_{17}$ compounds, finding the same linear dependence. This study of different R-Fe compounds corroborates that our proposed expression for B_{tR} provides a better description of the experimental data than the earlier proposed modeling of B_{tR}, which assumed that the rare earth polarization propagates via the RKKY mechanism.

Finally, the variation in B_{anis} in the nonaxial magnetic phases has been estimated, and the obtained values are consistent with the variation of μ_{orb} which appear at the SRT of $Nd_2Fe_{14}B$.

ACKNOWLEDGMENTS

Elias Palacios is thanked for his help in the dipolar field calculations. This work was financed by the MAT 02/166 and MAT 2000/0107/P4-02 MCYT projects (Spanish government). C.P. thanks MCYT for financial Grant No. PN73195091Y.

*Electronic address: cpiquer@unizar.es

[1] K. H. J. Buschow, Rep. Prog. Phys. **54**, 1123 (1991).
[2] H. Li and J. M. D. Coey, in *Handbook of Magnetic Materials*, Vol. 6, edited by K. H. J. Buschow (Elsevier Science, Amsterdam, 1991), p. 1.
[3] K. H. J. Buschow, in *Materials Science and Technology Series*, Vol. 3B, Part II, edited by K. H. J. Buschow (VCH Publishing, Berlin, 1994), p. 451.
[4] C. Piquer, M. Artigas, J. Rubín, and J. Bartolomé, J. Phys.: Condens. Matter **10**, 11055 (1998).
[5] M. Artigas, C. Piquer, J. Rubín, and J. Bartolomé, J. Magn. Magn. Mater. **196-197**, 653 (1999).
[6] C. Piquer, E. Palacios, M. Artigas, J. Bartolomé, J. Rubín, J. Campo, and M. Hofmann, J. Phys.: Condens. Matter **12**, 2265 (2000).
[7] Th. Sinnemann, M. U. Wisniewski, M. Rosenberg, and K. H. J. Buschow, J. Magn. Magn. Mater. **83**, 259 (1990).
[8] G. J. Bowden, D. S. P. Bunbury, A. P. Guimarăes, and R. E. Snyder, J. Phys. C **1**, 1376 (1968).
[9] P. Raj and S. K. Kulshreshtha, J. Phys. (Paris) **41**, 1487 (1980).
[10] C. Meyer, F. Hartmann-Boutron, Y. Gros, Y. Berthier, and J. L. Buevoz, J. Phys. (Paris) **42**, 605 (1981).
[11] F. Grandjean and G. J. Long, in *Interstitial Intermetallic Alloys. NATO ASI Series, Series E: Applied Sciences*, Vol. 281, edited by F. Grandjean, G. J. Long, and K. H. J. Buschow (Kluwer Academic Publishers, Dordrecht, 1995), p. 463.
[12] D. Hautot, G. J. Long, F. Grandjean, O. Isnard, and S. Miraglia, J. Appl. Phys. **86**, 220 (1999).
[13] T. Mazet and B. Malaman, J. Phys.: Condens. Matter **12**, 1085 (2000).
[14] C. Piquer, R. Hermann, F. Grandjean, G. J. Long, and O. Isnard, J. Appl. Phys. **93**, 3414 (2003).
[15] C. Piquer, F. Grandjean, G. J. Long, and O. Isnard, J. Alloys Compd. **353**, 33 (2003).
[16] C. Piquer, O. Isnard, F. Grandjean, and G. J. Long, J. Magn. Magn. Mater. **265**, 156 (2003).
[17] C. Piquer, R. Hermann, F. Grandjean, O. Isnard, and G. J. Long, J. Phys.: Condens. Matter **15**, 7395 (2003)
[18] C. Piquer, F. Grandjean, O. Isnard, V. Pop, and G. J. Long, J. Alloys Compd. **377**, 1 (2004).
[19] C. Piquer, F. Grandjean, O. Isnard, V. Pop, and G. J. Long, J. Appl. Phys. **95**, 6308 (2004).
[20] D. P. Lazar, N. Plugaru, V. Kuncser, M. Valeanu, G. Filoti, J. Bartolomé, and J. Rubín, J. Magn. Magn. Mater. **302**, 56 (2006).
[21] J. J. Bara, B. F. Bogacz, A. T. Pędziwiatr, P. Stefański, A. Szlaferek, and A. Wrzeciono, J. Alloys Compd. **265**, 70 (1998).
[22] X. Bo-Ping Hu, X. Hong-Shuo Li, J. P. Gavigan, and J. M. D. Coey, J. Phys.: Condens. Matter **1**, 755 (1989).
[23] M. Morariu, D. P. Lazar, A. Galatanu, N. Plugaru, V. Kuncser, G. Filoti, G. Hilscher, and A. Kottar, J. Alloys Compd. **285**, 37 (1999).
[24] J. Ayres de Campos, J. M. Gil, P. J. Mendes, L. P. Ferreira, I. C. Ferreira, N. Ayres de Campos, P. Estrela, M. Godinho, M. Bououdina, A. Collomb, D. Fruchart, J. L. Soubeyroux, S. Takele, J. Pelloth, and R. A. Brand, J. Magn. Magn. Mater. **164**, 305 (1996).
[25] C. Christides, A. Kostikas, G. Zouganelis, V. Psyharis, X. C. Kou, and R. Grossinger, Phys. Rev. B **47**, 11220 (1993).
[26] Z. W. Li, X. Z. Zhou, and A. H. Morrish, J. Phys.: Condens. Matter **4**, 10409 (1992).
[27] I. A. Campbell, J. Phys. F: Met. Phys. **2**, L47 (1972).
[28] V. Psycharis and C. Christides, J. Phys.: Condens. Matter **15**,

7953 (2003).
[29] I. S. Tereshina, P. Gaczyński, V. S. Rusakov, S. A. Nikitin, W. Suski, N. V. Tristan, and T. Palewski, J. Phys.: Condens. Matter **13**, 8161 (2001).
[30] C. Piquer, O. Isnard, F. Grandjean, and G. J. Long, J. Magn. Magn. Mater. **263**, 235 (2003).
[31] C. Piquer, F. Grandjean, G. J. Long, and O. Isnard, J. Alloys Compd. **388**, 6 (2005).
[32] L. Gelato, J. Appl. Crystallogr. **14**, 141 (1981).
[33] O. Isnard and D. Fruchart, J. Alloys Compd. **265**, 70 (1998).
[34] Landolt-Börnstein, *New Series Group III, Magnetic Properties of Metals*, Vol. 19a, edited by M. Shiga (Springer-Verlag, Berlin, 1986), Chapter 1.4.1.5.
[35] N. N. Greenwood and T. C. Gibb, in *Mössbauer Spectroscopy*, edited by N. N. Greenwood and T. C. Gibb (Chapman and Hall, London, 1971).
[36] The quadrupole shift is sometimes defined as $\varepsilon = e^2qQ(3\cos^2\theta - 1)/2$, the difference in the splitting between lines 1 and 2, and the splitting between lines 5 and 6 of the magnetic spectra. The data presented in this work should be multiplied by four to compare with ε values obtained with this expression.
[37] P. A. Algarabel, M. R. Ibarra, J. Bartolomé, L. M. García, and M. D. Kuz'min, J. Phys.: Condens. Matter **6**, 10551 (1994).
[38] J. L. Wang, N. Tang, Y. P. Shen, D. Yang, B. Fuquan, G. H. Wu, F. M. Yang, F. R. de Boer, E. Brück, and K. H. J. Buschow, J. Appl. Phys. **91**, 2165 (2002).
[39] J. L. Wang, B. García-Landa, C. Marquina, M. R. Ibarra, F. M. Yang, and G. H. Wu, Phys. Rev. B **67**, 014417 (2003).
[40] J. L. Wang, S. J. Campbell, J. M. Cadogan, O. Tegus, and A. V. J. Edge, J. Phys.: Condens. Matter **17**, 3689 (2005).
[41] C. Abadía, P. A. Algarabel, B. García-Landa, M. R. Ibarra, A. del Moral, N. V. Kudrevatykh, and P. E. Markin, J. Phys.: Condens. Matter **10**, 349 (1998).
[42] M. T. Averbuch-Pouchot, R. Chevalier, J. Deportes, B. Kebe, and R. Lemaire, J. Magn. Magn. Mater. **68**, 190 (1987).
[43] M. Kawakami, T. Hihara, Y. Koi, and T. Wakiyama, J. Phys. Soc. Jpn. **33**, 1591 (1972).
[44] R. H. Herber, in *Chemical Mössbauer Spectroscopy*, edited by R. H. Herber (Plenum Press, New York, 1984), p. 199.
[45] G. J. Long, D. Hautot, F. Grandjean, D. T. Morelli, and G. P. Meisner, Phys. Rev. B **60**, 7410 (1999).
[46] F. Grandjean, O. Isnard, and G. J. Long, Phys. Rev. B **65**, 064429 (2002).
[47] G. J. Long, O. Isnard, and F. Grandjean, J. Appl. Phys. **91**, 1423 (2002).
[48] R. Coehoorn, C. J. M. Denissen, and R. Eppenga, J. Appl. Phys. **69**, 6222 (1991).
[49] C. Lin, G. Z. Li, Z. X. Liu, H. W. Jiang, Z. Wan, J. L. Yang, B. S. Zhang, and Y. F. Ding, J. Appl. Phys. **70**, 6543 (1991).
[50] J. Hu, L. M. Mei, H. Li, Z. Y. Liu, J. L. Wang, and Q. F. Lin, Solid State Commun. **101**, 635 (1997).
[51] T. Sinnemann, K. Erdmann, M. Rosenberg, and K. H.J. Buschow, Hyperfine Interact. **50**, 675 (1989).
[52] W. G. Haije, J. Spijkerman, F. R. de Boer, K. Bakker, and K. H. J. Buschow, J. Less-Common Met. **162**, 285 (1990).
[53] M. Anagnostou, E. Devlin, V. Psycharis, A. Kostikas, and D. Niarchos, J. Magn. Magn. Mater. **131**, 157 (1994).
[54] T. Beuerle and M. Fähnle, J. Magn. Magn. Mater. **110**, L29 (1992).
[55] D. P. E. Dickson, in *Mössbauer Spectroscopy*, edited by D. P. E. Dickson and F. J. Berry (Cambridge University Press, Cambridge, 1986), Chapter 1, p. 11.
[56] V. A. Niculescu, T. J. Burch, and J. I. Budnick, J. Magn. Magn. Mater. **39**, 223 (1983).
[57] S. Blügel, H. Akai, R. Zeller, and P. H. Dederichs, Phys. Rev. B **35**, 3271 (1987).
[58] J. M. D. Coey, in *Rare-Earth Iron Permanent Magnets*, edited by J. M. D. Coey (Oxford Science Publications, Oxford, 1996), Chapter 1, p. 23.
[59] R. Coehoorn, J. Magn. Magn. Mater. **159**, 55 (1996).
[60] M. Morales, M. Bacmann, C. Baudelet, A. Delobbe, D. Fruchart, Ch. Giorgetti, G. Krill, and P. Wolfers, J. Alloys Compd. **317** 470 (2001).
[61] L. M. García, J. Chaboy, F. Bartolomé, and J. B. Goedkoop, Phys. Rev. Lett. **85**, 429 (2000).
[62] W. D. Brewer, A. Scherz, C. Sorg, H. Wende, K. Baberschke, P. Bencok, and S. Frota-Pessoa, Phys. Rev. Lett. **93**, 077205 (2004).
[63] H. Ebert, P. Strange, and L. B. Gyorffy, J. Phys. F: Met. Phys. **18**, L135 (1986).
[64] R. S. Preston, J. Heberle, and S. S. Hanna, Phys. Rev. **128**, 2207 (1962).
[65] C. T. Chen, Y. U. Idzerda, H. J. Lin, N. V. Smith, G. Meigs, E. Chaban, G. H. Ho, E. Pellegrin, and F. Sette, Phys. Rev. Lett. **75**, 152 (1995).
[66] I. A. Al-Omari, S. S. Jaswal, A. S. Fernando, D. J. Sellmyer, and H. H. Hamdeh, Phys. Rev. B **50**, 12665 (1994).
[67] J. M. D. Coey, A. Yaouanc, and D. Fruchart, Solid State Commun. **58**, 413 (1986).
[68] D. Hautot, G. J. Long, F. Grandjean, O. Isnard, and S. Miraglia, J. Appl. Phys. **86**, 2200 (1999).
[69] D. Hautot, G. J. Long, F. Grandjean, O. Isnard, and D. Fruchart, J. Magn. Magn. Mater. **202**, 107 (1999), and references therein.
[70] F. Grandjean, O. Isnard, D. Hautot, and G. J. Long, Phys. Rev. B **63**, 014406 (2001).
[71] G. J. Long, O. Isnard, and F. Grandjean, J. Appl. Phys. **91**, 1423 (2002).
[72] O. Isnard, D. Hautot, G. J. Long, and F. Grandjean, J. Appl. Phys. **88**, 2750 (2000).
[73] F. Grandjean, G. J. Long, O. A. Pringle, and J. Fu, Hyperfine Interact. **62**, 131 (1990).
[74] F. Grandjean and G. J. Long, in *Supermagnets, Hard Magnetic Materials*, edited by G. J. Long and F. Grandjean (Kluwer Academic Publishers, Amsterdam, 1991), Chapter 14.
[75] N. Plugaru, J. Rubín, J. Bartolomé, C. Piquer, and M. Artigas, Phys. Rev. B **65**, 134419 (2002).
[76] D. Fruchart, P. Wolfers, S. Miraglia, L. Pontonnier, F. Vaillant, H. Vicent, D. Le Roux, A. Yaouanc, P. Dalmas de Reotier, Ph. L'Héritier, and R. Fruchart, in *Concerted European Action on Magnets (CEAM)*, edited by I. V. Mitchell *et al.* (Elsevier, New York, 1988), p. 214.
[77] F. Grandjean, D. Hautot, G. J. Long, O. Isnard, S. Miraglia, and D. Fruchart, J. Appl. Phys. **85**, 4654 (1999).
[78] I. S. Tereshina, S. A. Nikitin, J. Stepien-Damm, W. Suski, A. A. Salamova, and V. N. Verbetsky, J. Magn. Magn. Mater. **258**, 427 (2003).
[79] D. P. Yang, J. I. Budnick, W. A. Hines, and Y. D. Zhang, J. Appl. Phys. **85**, 4651 (1999).